Electromagnetic and Statistical Approach to Improve Radar Performance in Multipath Environments

BY

HARUN TAHA HAYVACI
B.A., Bilkent University, Ankara, Turkey, 2005
M.S., University of Illinois at Chicago, Chicago, IL, USA, 2010

THESIS

Submitted as partial fulfillment of the requirements
for the degree of Doctor of Philosophy in Electrical and Computer Engineering
in the Graduate College of the
University of Illinois at Chicago, 2012

Chicago, Illinois

Defense Committee:

Danilo Erricolo, Chair and Advisor
Rashid Ansari
Natasha Devroye
Pawan Setlur
Piergiorgio L. E. Uslenghi
Antonio De Maio, Universita di Napoli, Italy
Traian Dogaru, U.S. Army Research Laboratory

To my parents Abdullah and Turkan, my wife Zeynep and our daughter Elif, that this thesis would not be completed without their continuos support and comfort.

ACKNOWLEDGMENTS

This dissertation would not have been possible without the guidance and the help of several individuals who in one way or another contributed and extended their valuable assistance in the preparation and completion of this study.

First I would like thank my advisor Prof. Danilo Erricolo whose guidance and encouragement I will never forget. He has always been very kind and supportive through this track that I admire him much. Second I would like to thank Prof. Antonio De Maio for his expertise and encouragement that also makes this thesis completed. I also welcome this opportunity to formally thank Prof. Natasha Devroye and Dr. Pawan Setlur for their guidance and expertise. I would like also to express my appreciation for the time and expertise of the committee members: Prof. Piergiorgio Uslenghi, Prof. Rashid Ansari and Dr. Traian Dogaru.

My profound thanks to my family: To my parents Abdullah and Turkan Hayaci, who have always dedicated themselves to be perfect parents to their children and taught us to be just and dedicated to do good. They have always been and will always be a source of inspiration and ultimate role model for me. I always feel granted by their trust and support. I would not be here without their guidance and wisdom. To my in-laws Fehmi and Nebahat Koru for their enormous support and guidance. Their knowledge and wisdom always enlighten my path. To my brothers and sisters: Emin and Kamer, Fatma and Deniz, Zehra, Mehmet, Sirin, Ahmet, and Omer for their prayers and support. They have always come to our help when we need it. To my grandparents, aunts and uncles for their prayers. To my cousin Ergun who has become

an elder brother for me in Chicago. To friends, whom I consider as part of my family, for their support and sharing my happiness and pride on the completion of this dissertation.

Last but not the least, very special thanks to my lovely wife Zeynep, who has shown not only extraordinary patience but also great support and contribution on this track. My all success belongs to her too. She and my daughter Elif, who is the most precious gift God has given us, have always been and will always be the source of my happiness and comfort. Elif deserves special thanks for being a nice girl while I and her mom were studying. She sacrificed the most.

HTH

PREFACE

In this work, multipath exploitation in radar target detection and parameter estimation is considered. Multipath is a natural phenomenon present in almost every propagation environment and affects radar problems such as urban area sensing, through the wall radar imaging, and low altitude target detection and parameter estimation. In the past thirty years multipath has been viewed as a negative effect that needs to be mitigated; researchers have developed many signal processing techniques in that regard. Recently however, our view on multipath is changing: with the proper knowledge of the environment, multipath may be considered to be an opportunity to obtain additional degrees of freedom by providing virtual radar sensors that observe the target from different aspects. Thus, multipath exploitation has been receiving more interest lately in order to achieve more robust performance and degrees of freedom in detection and estimation problems. Although there is strong evidence that one can improve detection and estimation performance in radar through multipath exploitation, the amount of improvement still depends on the radar-target geometry, the corresponding multipath structure and the available signal noise ratio (SNR) levels. Thus, a quantitative analysis of the target probability of detection and parameter estimation accuracy with and without multipath exploitation, the topic of this thesis, is needed in order to fully assess the performance improvement.

TABLE OF CONTENTS

TABLE OF CONTENTS (Continued)

CHAPTER **PAGE**

LIST OF FIGURES

LIST OF FIGURES (Continued)

FIGURE **PAGE**

LIST OF ABBREVIATIONS

AoA	Angle of arrival
BW	Bandwidth
CCDF	Complementary cumulative distribution function
CFAR	Constant False Alarm Rate
CRLB	Cramér Rao Lower Bound
CWGN	Complex white Gaussian Noise
DARPA	Defense Advanced Research Projects Agency
SNR	Signal to noise ratio
EM	Electromagnetics
FIM	Fisher Information Matrix
GMTI	Ground moving target indicator
GLRT	Generalized Likelihood Ratio Test
GPS	Global Positioning System
H_1	Hypothesis of target presence
H_0	Hypothesis of target absence
LoS	Line of sight
MER	Multipath Exploitation Radar

LIST OF ABBREVIATIONS (Continued)

ML	Maximum Likelihood
MLE	Maximum Likelihood Estimation
MSE	Mean Squared Error
NP	Neyman Pearson
OFDM	Orthogonal Frequency Division Multiplexing
PSD	Power spectral density
RCS	Radar Cross Section
SAR	Synthetic aperture radar
UIC	University of Illinois at Chicago
UMP	Uniformly most powerful

LIST OF SYMBOLS

a	Scalar quantity
$\tilde{a}$	Complex scalar quantity
$\mathbf{A}$	Vector quantity
$< \cdot >$	Scalar product in the L^2 space
$\lvert \cdot \rvert$	Modulus
T	Transpose
†	Complex conjugate transpose
$\Re$	Real part
$Q(\cdot)$	Complementary cumulative distribution function
$Q^{-1}(\cdot)$	Inverse complementary cumulative distribution function
χ^2_k	Central Chi-square distribution with k degree of freedom
$\chi^2_k(\lambda)$	Non-central Chi-square distribution with k degree of freedom and non centrality parameter λ
P_D	Probability of detection
P_{FA}	Probability of false alarm

LIST OF SYMBOLS (Continued)

$\mathbf{J}$	Fisher information matrix
E	Statistical expectation operator
Var	Variance

SUMMARY

In this thesis, a novel approach is presented to evaluate the performance improvement of a radar system exploiting multipath, as compared to a conventional system that exploits only the direct path return. This novel approach to exploit multipath requires prior knowledge of the radar target environment.

In Chapter 2, time delay estimation using the maximum likelihood principle is addressed for the multipath exploitation problem and the corresponding Cramér-Rao bounds are derived. A single wideband radar and a target in a known reflecting geometry are assumed. If the multipath is indeed detectable and resolvable, it is show that multipath exploitation permits estimating the angle of arrival (AoA) of the target with a single sensor and improves estimation accuracy of the direct path time delay. These are both possible because the multipath time delay is a deterministic function of the time delay of the direct path as well as its AoA, as it is demonstrated here. The multipath caused from reflections from surfaces yields virtual radar sensors observing the target from different aspects, thereby allowing AoA estimation.

In Chapter 3, a new method to address radar target detection problems in multipath environments is considered. The novelty of the proposed method is that it exploits prior knowledge on the environment and combines it with electromagnetic modeling to determine some information about the possible multipath structure. This information is used to separate the environment into different regions based upon the behavior of the multipath components. Specifically, as a case study, we consider a radar and a target in the presence of a reflecting ground. For this

environment, three regions are determined based upon the amount of overlap among the multipath components. For each region, receivers are designed exploiting the multipath structure. Thus, a different viewpoint to analyze radar detection problems is suggested. The two main results are the improvement in the target probability of detection, by properly accounting for the multipath, and the a priori determination of the best performing detector based upon the location of the target and the available signal-to-noise ratio.

CHAPTER 1

INTRODUCTION

1.1 Motivation and Background Work

In radar problems, the effect of the surrounding environment has been widely studied and well understood through advanced Electromagnetic (EM) modeling (1), (2). However detection and estimation problems are still challenging in environments with a rich multipath structure such as those present in urban area sensing and through the wall radar imaging applications. This situation is due to the lack of integration between signal processing and EM modeling of the environment under consideration. Diversity is considered to be one appropriate method in which one can deal with multipath (3). In particular, with adaptive radars, it has been well understood that prior knowledge of the environment and its effective parameters may be used to enhance the detection, estimation and tracking performance of radar systems (4)-(11). Recently, with the development of advanced and computationally efficient EM tools, EM propagation models and simulations are being incorporated into radar and sensing problems as well (12)-(15). Along these lines, this work investigates the problem of target detection and estimation in a multipath environment. Our work considers diverse receiving strategies which improve their performance by exploiting prior knowledge of the radar-target environment through advanced EM modeling.

Multipath is a natural phenomenon present in almost every propagation environment and affects radar problems, particularly those involving urban area sensing, through the wall radar imaging, and low altitude target detection and parameter estimation. In the past thirty years multipath has been viewed as a negative effect that needs to be mitigated; researchers have developed many signal processing techniques in that regard. Multipath may degrade the detection and estimation (of a target) performance in radar systems unless it is properly accounted for. Through the years, several approaches have been presented that aim to diminish the effects of multipath (16)-(19) and the references therein. In (19) Lo and Litva introduced the prior information in the Maximum Likelihood, ML, process to enhance the ML estimator performance. The key feature of their approach is the use of a highly deterministic multipath signal model.

However, some researchers consider multipath to be an opportunity for obtaining more degrees of freedom about the system by providing virtual radar sensors that observe the target from different aspects. Bossé *et al.* have considered exploiting multipath information with a deterministic specular multipath model for better tracking accuracy (20), (21). Sherman first modeled the multipath interference pattern for low-angle tracking with a technique called "complex indicated angle" (22), (23). The multipath exploitation problem has been studied in the recent past as well in, *e.g.* (24) -(40), and references therein. Recently, the Defense Advanced Research Projects Agency (DARPA) had initiated the Multipath Exploitation Radar (MER) program to that aims to extend the coverage of airborne sensors by using the signals reflected off the building in urban areas (24). Authors of (25) first provided the probabilities of line-of-sight (LoS) and non-line-of-sight (NLoS) visibility of a target in a given multipath

environment and evaluated the potential of multipath exploitation to increase the radar coverage area and to improve the detection of moving targets in dense urban areas. Later, in (26) the authors exploited multipath in the absence of the direct path return in ground moving target indicator (GMTI) radar to detect and track ground targets in urban areas. The same authors conducted a controlled outdoor experiment to collect X-band radar data to validate the predicted multipath response, and the received multipath power in relation to the LoS response (27). In their work, it is also emphasized that knowledge-based methods can be utilized to either coherently or non-coherently process multipath returns, beyond the standard GMTI processing, with the prior knowledge of the urban geometry. Furthermore, in (28) it is shown that dismount classification, tracking, and localization of humans walking in an urban environment can be enhanced via multipath exploitation when both direct and reflected path returns are available. In (34) the authors demonstrated experimentally that indoor targets, *i.e.* rotating fans and a walking person with metal reflectors, are detected via NLoS multipath returns. The multipath exploitation paradigm is also integrated with adaptive waveform design to enhance the target tracking capabilities and performance of a radar (29). A multipath model and exploitation technique is addressed in (32), which properly utilizes the target ghosts in through-the-wall and urban radar sensing applications. Using the multipath exploitation, authors of (33) also demonstrated that localization can be achieved with a single sensor. In (35) a bistatic synthetic aperture radar (SAR), which exploits multipath, is used for an imaging scenario in a multipath environment where the final image of the target is obtained via coherent superposition of multiple reconstructed images.

This thesis considers radar target detection and parameter estimation in a multipath environment. Multipath is a natural phenomenon present in most propagation environments such as in urban areas and in low-angle radar target detection problems. Recently, multipath exploitation has been receiving more interest in radar problems in order to achieve more robust performance and degrees of freedom in detection and estimation problems (29)-(40). Although there is strong evidence that one can improve the detection and estimation performance in radar through multipath exploitation, the amount of improvement still depends on the radar-target geometry, the available SNR levels, the bandwidth (BW) and the correlation of mulltipath returns (36). Thus, a quantitative analysis of the target probability of detection and accuracy of parameter estimation with and without multipath exploitation is needed in order to fully assess the performance improvements.

1.2 Organization

In Chapter 2, the time delay estimation using the maximum likelihood principle is addressed for the multipath exploitation problem and corresponding Cramér-Rao bounds are derived. A single wideband radar and a target in a known reflecting geometry are assumed. If the multipath is indeed detectable and resolvable, it is shown that multipath exploitation permits estimating the AoA of the target with a single sensor and improves the estimation accuracy of the direct path time delay. Both these are possible because the time delay of the reflected path is a deterministic function of the time delay of the direct path as well as its AoA, as it is demonstrated here. The multipath caused from reflections from surfaces yields virtual radar sensors observing the target from different aspects, thereby allowing AoA estimation.

In Chapter 3, we consider a basic case study to show how to conduct an electromagnetic (EM) analysis that takes advantage of the prior knowledge of the environment where the radar operates. As a result, we obtain the propagation time of each multipath component. Then, the propagation time information is used to partition the environment into regions where diverse receiving strategies are applied. The criterion to determine the regions is the amount of overlap, in the time-domain, of the multipath components of the received signal. The amount of overlap depends on the environment, locations of the radar and the target, and the duration of the transmitted pulse. Accordingly, the general received signal model is specialized within each region to account for the presence of significant overlap or its absence. Then, within each region, a different receiver is devised thus justifying the statement of diverse receiving strategies. Neyman-Pearson tests (NP) as optimum detectors, and Generalized Likelihood Ratio Tests (GLRT) as sub-optimum detectors are devised for each region.

1.3 Research Contribution

A method is provided to increase the target detection and parameter estimation performance of a radar in a multipath environment. The method exploits prior knowledge of the environment and, through an appropriate EM modeling, integrates it into a statistical signal processing framework. A qualitative analysis of the improvement in the target detection and parameter estimation via multipath exploitation is provided. The proposed method is illustrated in a basic case study scenario, however the approach is quite general and it could be extended to more complex environments.

CHAPTER 2

MAXIMUM LIKELIHOOD TIME DELAY ESTIMATION AND CRAMÉR-RAO BOUNDS FOR MULTIPATH EXPLOITATION

2.1 Introduction

The objective in multipath exploitation radar is improving the radar system performance by incorporating the additional information, about either targets or their environments, embedded in the multipath returns. The multipath exploitation hypothesis rests on the fact that "multipath exists because of the environment," which in turn requires that multipath returns are distinguishable.

In this chapter, a single wideband radar sensor observes a target in *a priori* known reflecting geometry, consisting of a ground plane. Accordingly, the multipath returns are caused by specular reflections of the radar signal from a smooth surface, an assumption seen for example in (29)-(40) and references therein.

The novelty of this approach is that, using a ray tracing analysis (49), the multipath time delay is parameterized as a function of the geometrical direct path time-delay and its AoA; in particular, this approach is applicable even when the direct path is obstructed. Since multipath time delay on its own is not directly useful, by employing this parametrization, the maximum likelihood estimator (MLE) and the Cramér-Rao lower bounds (CRLB) are derived for esti-

mating the direct path time delay as well as its AoA. The CRLBs are derived in the frequency domain, and are shown to be a function of the SNR as well as the operating bandwidth.

The multipath exploitation problem has been studied in the recent past in, *e.g.* (26)-(38), and references therein. In (27), the authors conducted a controlled outdoor experiment to collect X-band radar data to validate the predicted multipath response, and the received multipath power in relation to the LoS response. In their work, they also emphasized that knowledge-based methods can be utilized to either coherently or non-coherently process multipath returns, beyond the standard GMTI processing, with the prior knowledge of the urban geometry. In (36)-(38), detection using the generalized likelihood ratio test (GLRT) was employed for the multipath exploitation problem, assuming the knowledge of the reflected and direct path time delays, obtained from a priori knowledge of the environment where the radar operates. A multipath model and exploitation technique, which properly utilizes the target ghosts in through-the-wall and urban radar sensing applications, is addressed in (32). Using multipath exploitation, the authors of (33) demonstrated that localization can be achieved with a single sensor. Examples of targets in urban canyons and through-the-wall radar were employed to demonstrate non-coherent localization. Target tracking and ground moving target indication (GMTI) applications of exploitation were explored in (29) and (25), respectively.

This chapter is organized as follows, in Section II the model is presented, and in Section III the problem is presented formally. The maximum likelihood (ML) technique and the CRLB are presented in Sections VI and V, respectively. Representative simulation results and conclusions are presented in Section VI and VII.

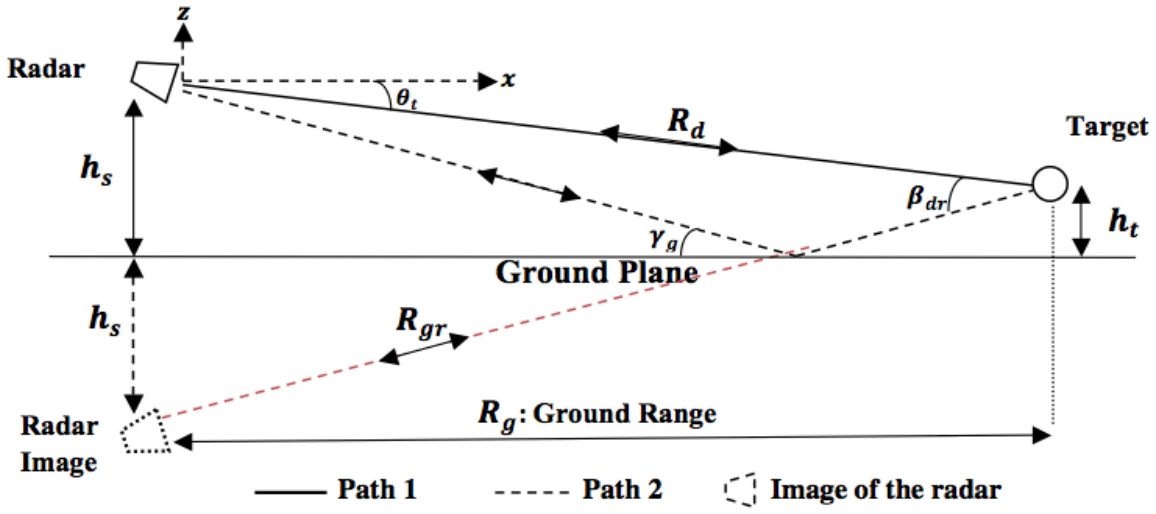

Figure 1. Geometry of the problem: Radar-Target over a Ground Plane

2.2 Multipath Propagation Model

In this Section we describe the sample radar-target scenario that involves multipath propagation. The geometry of the radar-target environment is illustrated in Figure 1. We formulate the mathematical expression for the propagation model of the radar scene using ray-tracing techniques. The advantage of the ray-tracing approach is that each individual trajectory is explicitly associated with all the mechanisms of wave propagation so that a clear description of all the physical phenomena is available (49). A two-ray model is considered at first to remain

tractable. The radar is assumed to be located at the origin of a polar coordinate system. The transmitted pulse is assumed to be

$$s(t) = \begin{cases} \frac{1}{\sqrt{T_d}} & 0 \leq t \leq T_d \\ 0 & \text{otherwise} \end{cases}$$

so that the received signal is given as

$$r_t = \sum_{i=1}^{2} \tilde{\alpha}_i(t) s(t - \tau_i) + \tilde{w}(t)$$

where r_t, $s(t)$ and $\tilde{w}(t)$ are the baseband equivalents of the received signal, transmitted signal and noise, respectively. Parameters $\tilde{\alpha}_1(t)$ and $\tilde{\alpha}_2(t)$, which are complex and deterministic, are the strengths of the direct and reflected multipath returns, of time delays τ_1 and τ_2, respectively.

2.3 Problem Formulation

In this section, we assume $\tilde{w}(t)$ is a stationary zero-mean complex circular white Gaussian random process with power spectral density σ^2. Since the pulse duration, T_d, is considered small compared to the coherence time of the radar-target channel, $\tilde{\alpha}_1(t)$ and $\tilde{\alpha}_2(t)$ are approximated with unknown complex deterministic parameters $\tilde{\alpha}_1$ and $\tilde{\alpha}_2$, respectively. Then, r_t can be written as, (36),

$$r_t = \sum_{i=1}^{2} \tilde{\alpha}_i s(t - \tau_i) + \tilde{w}(t).$$

In terms of geometric parameters, the time delays τ_1 and τ_2 are obtained as

$$\tau_1 = \frac{2R_d}{c} \quad \text{and} \quad \tau_2 = \frac{2R_{gr}}{c},$$

where R_d and R_{gr} are the ranges of target with respect to the radar and radar image respectively. Furthermore τ_2 can be written as a function of τ_1 and θ_t with *a priori* knowledge of h_s, which is the height of the radar from the planar reflecting surface.

$$\tau_2 = g(\tau_1, \theta_t) = \sqrt{(\tau_1 \cos\theta_t)^2 + (4h_s/c + \tau_1 \sin\theta_t)^2}.$$

Thus, for the estimation problem, the received signal can be written as

$$\begin{aligned} r_t &= \tilde{\alpha}_1 s(t - \tau_1) + \tilde{\alpha}_2 s(t - g(\tau_1, \theta_t)) + \tilde{w}(t) \\ &= \tilde{s}_1(t,\ \mathbf{\Theta}) + \tilde{s}_2(t,\ \mathbf{\Theta}) + \tilde{w}(t), \end{aligned}$$

where $t \in [0, T_o]$ is the observation interval and $\mathbf{\Theta} := [\tau_1, \theta_t, \tilde{\alpha}_1, \tilde{\alpha}_2]^T$ is the vector of parameters to be estimated. It should be noted that $\mathbf{\Theta}$ includes both real and complex parameters.

The novelty of this approach is that we estimate two geometrical parameters, $[\tau_1, \theta_t]^T$ with a single sensor by exploiting the multipath and *a priori* knowledge of the reflecting environment. In other words, h_s is assumed to be known.

2.4 Maximum Likelihood Estimation

The MLE formulation adopted here is similar to the one taken in (50), but unlike our approach, the authors of (50) estimate the multipath time delay for multipath mitigation in

global positioning systems (GPS). The log-likelihood function that needs to be maximized with respect to $\mathbf{\Theta}$, and is readily shown to be

$$\ln \mathbf{\Lambda}[r_t, \mathbf{\Theta}] \propto -\frac{2}{\sigma^2} \int_0^{T_o} \left| r_t - \sum_{i=1}^{2} \tilde{s}_1(t, \mathbf{\Theta}) \right|^2 dt \tag{2.1}$$

In general, for an efficient unbiased estimator we must have (51), (52),

$$\frac{\partial \ln \mathbf{\Lambda}[r_t, \mathbf{\Theta}]}{\partial \Theta_i} = [\widehat{\Theta}_i(r_t) - \Theta_i] J_{ii}(\Theta_i), \tag{2.2}$$

where J_{ij} is the (i, j)-th element of the Fisher information matrix (FIM) $\mathbf{J}$ as in Equation 2.4, $\widehat{\Theta}_i$ is the i-th element of the estimator vector $\widehat{\mathbf{\Theta}}$ which is a function of the received data, whereas Θ_i is the i-th element of unknown parameter vector $\mathbf{\Theta}$. In this particular problem, the equality in Equation 2.2 does not hold for time-delay τ_1 and angle of arrival θ_t estimation but only for $\tilde{\alpha}_1$ and $\tilde{\alpha}_2$ (51), (52). Nevertheless, the maximum likelihood estimation is considered here due to its asymptotically efficient properties.

As a comparison point, we recall the celebrated Cramér-Rao inequality

$$Var\left(\hat{\Theta}_{ij}(r_t) - \Theta_{ij}\right) \geq J^{ij} \tag{2.3}$$

where J^{ij} is defined as the (i,j)-th element of the square matrix $\mathbf{J}^{-1}$ which is the inverse of the FIM $\mathbf{J}$. Elements of $\mathbf{J}$ are defined as, (51),

$$\mathbf{J} = -E\left\{\frac{\partial^2 \ln \mathbf{\Lambda}[r_t, \mathbf{\Theta}]}{\partial \mathbf{\Theta} \partial \mathbf{\Theta}^T}\right\} \tag{2.4}$$

where $E\{\cdot\}$ denotes the statistical expectation operator.

2.5 MLE of Amplitudes

From equation Equation 2.1, the MLE scores for $\tilde{\alpha}_1$ is obtained as

$$\begin{aligned}\frac{\partial \ln \mathbf{\Lambda}[r_t, \mathbf{\Theta}]}{\partial \tilde{\alpha}_1} &= \frac{\partial}{\partial \tilde{\alpha}_1}\left[-\frac{1}{\sigma^2}\int_0^{T_0}\left|r_t - \sum_{i=1}^{2}\tilde{s}_i(t,\mathbf{\Theta})\right|^2 dt\right] \\ &= \frac{1}{\sigma^2}\int_0^{T_0} s(t-\tau_1)\left(r_t - \sum_{i=1}^{2}\tilde{s}_i(t,\mathbf{\Theta})\right)dt \\ &= \frac{1}{\sigma^2}\left[\tilde{R}_{rs}(\tau_1) - \tilde{\alpha}_1^* - \tilde{\alpha}_2^*\Phi(\tau_1,\tau_2)\right].\end{aligned} \tag{2.5}$$

and, similarly, the MLE score for $\tilde{\alpha}_2$ is

$$\begin{aligned}\frac{\partial \ln \mathbf{\Lambda}[r_t, \mathbf{\Theta}]}{\partial \tilde{\alpha}_2} &= \frac{\partial}{\partial \tilde{\alpha}_2}\left[-\frac{1}{\sigma^2}\int_0^{T_0}\left|r_t - \sum_{i=1}^{2}\tilde{s}_i(t,\mathbf{\Theta})\right|^2 dt\right] \\ &= \frac{1}{\sigma^2}\int_0^{T_0} s(t-\tau_2)\left(r_t - \sum_{i=1}^{2}\tilde{s}_i(t,\mathbf{\Theta})\right)dt \\ &= \frac{1}{\sigma^2}\left[\tilde{R}_{rs}(\tau_2) - \tilde{\alpha}_2^* - \tilde{\alpha}_1^*\Phi(\tau_1,\tau_2)\right],\end{aligned} \tag{2.6}$$

where

$$\tilde{R}_{rs}(\tau) = \int_0^{T_o} r_t s^*(t-\tau)dt \tag{2.7}$$

$$\Phi(\tau_i, \tau_j) = \int_0^{T_o} s(t-\tau_i)s^*(t-\tau_j)dt. \tag{2.8}$$

Thus, the MLE equations to be solved for $\widehat{\tilde{\alpha}}_1$, and $\widehat{\tilde{\alpha}}_2$ are

$$\tilde{R}_{rs}(\tau_1) - \tilde{\alpha}_1^* - \tilde{\alpha}_2^*\Phi(\tau_2, \tau_1) = 0, \tag{2.9}$$

$$\tilde{R}_{rs}(\tau_2) - \tilde{\alpha}_2^* - \tilde{\alpha}_1^*\Phi(\tau_1, \tau_2) = 0. \tag{2.10}$$

We can represent and solve Equation 2.9 to Equation 2.10 by letting $\mathbf{R_{rs}} = [\tilde{R}_{rs}(\tau_1), \tilde{R}_{rs}(\tau_2)]^T$, $\mathbf{\Omega} = [\tilde{\alpha}_1, \tilde{\alpha}_2]^\dagger$, and

$$\mathbf{A} = \begin{pmatrix} 1 & \Phi(\tau_1, \tau_2) \\ \Phi(\tau_1, \tau_2) & 1 \end{pmatrix}. \tag{2.11}$$

Then the MLE equation becomes

$$\mathbf{R_{rs}} - \mathbf{A\Omega} = 0, \tag{2.12}$$

and can be easily solved as

$$\widehat{\mathbf{\Omega}} = \mathbf{A^{-1}R_{rs}}, \tag{2.13}$$

where $\widehat{\mathbf{\Omega}} = [\widehat{\tilde{\alpha}}_1, \widehat{\tilde{\alpha}}_2]^\dagger$. The $\widehat{\mathbf{\Omega}}$ is the unbiased efficient estimator that satisfy the equality given in Equation 2.2.

2.6 Estimation of Time Delay τ_1 and Angle of Arrival θ_t

In this section we derive the MLE equations for τ_1 and θ_t. In this case the estimation problem is not linear as it was in the amplitude estimation. Although there is no efficient unbiased estimator for τ_1 and θ_t, MLE can be implemented numerically and it is asymptotically unbiased and efficient.

The ML score for τ_1 is found as

$$\begin{aligned}\frac{\partial \ln \mathbf{\Lambda}[r_t, \mathbf{\Theta}]}{\partial \tau_1} &= -\frac{1}{\sigma^2}\int_0^{T_0} \frac{\partial}{\partial \tau_1}\Big| r_t - \sum_{i=1}^{2} \tilde{s}_i(t, \mathbf{\Theta})\Big|^2 dt \\ &= \frac{2}{\sigma^2}\Re\left\{\int_0^{T_o}\left\{r_t - \sum_{i=1}^{2}\tilde{s}_i(t,\mathbf{\Theta})\right\}\sum_{i=1}^{2}\frac{\partial \tilde{s}_i^*(t,\mathbf{\Theta})}{\partial \tau_1}dt\right\}.\end{aligned} \tag{2.14}$$

Thus, the MLE equation to be solved for $\widehat{\tau}_1$ is

$$\Re\left\{\int_0^{T_o}\left\{r_t - \sum_{i=1}^{2}\tilde{s}_i(t,\mathbf{\Theta})\right\}\sum_{i=1}^{2}\frac{\partial \tilde{s}_i^*(t,\mathbf{\Theta})}{\partial \tau_1}dt\right\} = 0. \tag{2.15}$$

In a similar manner, the MLE score for θ_t is found as

$$\begin{aligned}\frac{\partial \ln \mathbf{\Lambda}[r_t, \mathbf{\Theta}]}{\partial \theta_t} &= \int_0^{T_0} \frac{\partial}{\partial \theta_t} \Big| r_t - \sum_{i=1}^{2} \tilde{s}_i(t, \mathbf{\Theta}) \Big|^2 dt \\ &= \frac{2}{\sigma^2} \Re \left\{ \int_0^{T_o} \left\{ r_t - \sum_{i=1}^{2} \tilde{s}_i(t, \mathbf{\Theta}) \right\} \sum_{i=1}^{2} \frac{\partial \tilde{s}_i^*(t, \mathbf{\Theta})}{\partial \theta_t} dt \right\}.\end{aligned} \tag{2.16}$$

and the MLE equation to be solved for $\widehat{\theta}_t$ is

$$\Re \left\{ \int_0^{T_o} \left\{ r_t - \sum_{i=1}^{2} \tilde{s}_i(t, \mathbf{\Theta})] \right\} \sum_{i=1}^{2} \frac{\partial \tilde{s}_i^*(t, \mathbf{\Theta})}{\partial \theta_t} dt \right\} = 0. \tag{2.17}$$

There is no closed form expression for $\widehat{\tau}_1$ and $\widehat{\theta}_t$. However, one can obtain $\widehat{\tau}_{1_{ml}}$ and $\widehat{\theta}_{t_{ml}}$, respectively, by solving the equations Equation 2.15 and Equation 2.17 numerically.

In order to concentrate the likelihood function Equation 2.1 on τ_1 and θ_t we insert $\widehat{\tilde{\alpha}}_1$ and $\widehat{\tilde{\alpha}}_2$, which are given in Equation 2.13 into the likelihood function and maximize the resulting likelihood function, with respect to τ_1 and θ_t only, as

$$\max_{\tau_1, \theta_t} \Big(\ln \mathbf{\Lambda}[r_t, \mathbf{\Theta}] \Big) = \max_{\tau_1, \theta_t} \left(\frac{2}{\sigma^2} \int_0^{T_o} \left| r_t - \sum_{i=1}^{2} \widehat{\tilde{\alpha}}_i s(t - \tau_i) \right|^2 dt \right), \tag{2.18}$$

where

$$\tau_2 = g(\tau_1, \theta_t). \tag{2.19}$$

Closed form expressions for Equation 2.15-Equation 2.18 are intractable and the MLE must be evaluated numerically.

2.7 Cramér Rao Lower Bound

In this section the CRLB for the estimates of $\mathbf{\Theta} = [\tau_1, \theta_t, \alpha_1, \alpha_2]^T$ is derived. Here, we assume the perfect knowledge of the noise variance σ^2 and the phases of $\tilde{\alpha}_1$ and $\tilde{\alpha}_2$. α_1 and α_2 are the magnitudes of the complex amplitudes $\tilde{\alpha}_1$ and $\tilde{\alpha}_2$, respectively. Since $\mathbf{J}$ is block-diagonal matrix, having the perfect knowledge of σ^2 and phase of the complex amplitudes does not effect our CRLB analysis on the estimates of $\mathbf{\Theta} = [\tau_1, \theta_t, \alpha_1, \alpha_2]^T$. In order to assess the CRLB Equation 2.3 for the estimates, we compute elements of the FIM, $\mathbf{J}$, via Equation 2.4 and evaluate $\mathbf{J}^{-1}$ numerically.

For τ_1 we differentiate Equation 2.15 and take the expectation as

$$
\begin{aligned}
E\left[\frac{\partial^2 \ln \mathbf{\Lambda}[r_t, \mathbf{\Theta}]}{\partial \tau_1^2}\right] &= E\left[\frac{2}{\sigma^2}\Re\left\{\frac{\partial}{\partial \tau_1}\int_0^{T_o}\left\{r_t - \sum_{i=1}^{2}\tilde{s}_i(t,\mathbf{\Theta})\right\}\sum_{i=1}^{2}\frac{\partial \tilde{s}_i^*(t,\mathbf{\Theta})}{\partial \tau_1}dt\right\}\right] \\
&= E\left[\frac{2}{\sigma^2}\Re\left\{\int_0^{T_o} -\sum_{i=1}^{2}\frac{\partial \tilde{s}_i(t,\mathbf{\Theta})}{\partial \tau_1}\sum_{i=1}^{2}\frac{\partial \tilde{s}_i^*(t,\mathbf{\Theta})}{\partial \tau_1}dt\right\}\right] \\
&\quad + E\left[\frac{2}{\sigma^2}\Re\left\{\int_0^{T_o}\left\{r_t - \sum_{i=1}^{2}\tilde{s}_i(t,\mathbf{\Theta})\right\}\sum_{i=1}^{2}\frac{\partial^2 \tilde{s}_i^*(t,\mathbf{\Theta})}{\partial \tau_1^2}dt\right\}\right].
\end{aligned}
$$

In the second term one can observe that

$$
E\left[r_t - \sum_{i=1}^{2}\tilde{s}_i(t,\mathbf{\Theta})\right] = E\left[\tilde{w}(t)\right] = 0.
$$

The first term is a non-random term, thus

$$E\left[\frac{\partial^2 \ln \mathbf{\Lambda}[r_t, \mathbf{\Theta}]}{\partial \tau_1^2}\right] = -\frac{2}{\sigma^2}\int_0^{T_o}\left|\sum_{i=1}^{2}\frac{\partial \tilde{s}_i(t,\mathbf{\Theta})}{\partial \tau_1}\right|^2 dt.$$

In a similar manner,

$$E\left[\frac{\partial^2 \ln \mathbf{\Lambda}[r_t, \mathbf{\Theta}]}{\partial \theta_t^2}\right] = -\frac{2}{\sigma^2}\int_0^{T_o}\left|\sum_{i=1}^{2}\frac{\partial \tilde{s}_i(t,\mathbf{\Theta})}{\partial \theta_t}\right|^2 dt.$$

Then J_{11} and J_{22} can be written respectively as

$$J_{11} = -E\left[\frac{\partial^2 \ln \mathbf{\Lambda}[r_t, \mathbf{\Theta}]}{\partial \tau_1^2}\right] = \frac{2}{\sigma^2}\int_0^{T_o}\left|\sum_{i=1}^{2}\frac{\partial \tilde{s}_i(t,\mathbf{\Theta})}{\partial \tau_1}\right|^2 dt, \tag{2.20}$$

and

$$J_{22} = -E\left[\frac{\partial^2 \ln \mathbf{\Lambda}[r_t, \mathbf{\Theta}]}{\partial \theta_t^2}\right] = \frac{2}{\sigma^2}\int_0^{T_o}\left|\sum_{i=1}^{2}\frac{\partial \tilde{s}_i(t,\mathbf{\Theta})}{\partial \theta_t}\right|^2 dt. \tag{2.21}$$

It is also noted that J_{11} in Equation 2.20, which exploits multipath, is always greater than the FIM element J_{11} in (50), which considers the multipath to be independent of the direct path, and shown below

$$J_{11} = -E\left[\frac{\partial^2 \ln \mathbf{\Lambda}[r_t, \mathbf{\Theta}]}{\partial \tau_1^2}\right] = \frac{2}{\sigma^2}\int_0^{T_o}\left|\frac{\partial \tilde{s}_1(t,\mathbf{\Theta})}{\partial \tau_1}\right|^2 dt.$$

This implies that, for this geometry and assumptions, multipath exploitation improves the accuracy of τ_1 estimates, at least in the CRLB sense.

Through mathematical manipulations one can write J_{11} and J_{22} in a more explicit form, respectively, as

$$J_{11} = \frac{2}{\sigma^2}\Bigg\{ \left[|\tilde{\alpha}_1|^2 + |\tilde{\alpha}_2|^2 G_1^2\right] \int_{-\infty}^{\infty} (2\pi f)^2 |S(f)|^2 df + 2\Re\Bigg\{ \tilde{\alpha}_1 \tilde{\alpha}_2^* G_1 \int_{-\infty}^{\infty} (2\pi f)^2 e^{-j2\pi f(\tau_1 - \tau_2)} |S(f)|^2 df \Bigg\} \Bigg\} \tag{2.22}$$

and

$$J_{22} = \frac{2}{\sigma^2}\Bigg\{ \left[|\tilde{\alpha}_2|^2 G_2^2\right] \int_{-\infty}^{\infty} (2\pi f)^2 |S(f)|^2 \, df \Bigg\} \tag{2.23}$$

where

$$G_1 = \frac{\partial \tau_2}{\partial \tau_1} = \frac{\tau_1 + 4\sin\theta h_s/c}{\sqrt{\left(\tau_1 \cos\theta_t\right)^2 + \left(4h_s/c + \tau_1 \sin\theta_t\right)^2}},$$
$$G_2 = \frac{\partial \tau_2}{\partial \theta_t} = \frac{4h_s \tau_1 \cos\theta_t/c}{\sqrt{\left(\tau_1 \cos\theta_t\right)^2 + \left(4h_s/c + \tau_1 \sin\theta_t\right)^2}}.$$

Through Equation 2.9-Equation 2.8 we find the Fisher information matrix elements for α_1 and α_2 as

$$J_{33} = -E\left[\frac{\partial^2 \ln \mathbf{\Lambda}[r_t, \mathbf{\Theta}]}{\partial \alpha_1^2}\right] = \frac{2}{\sigma^2}, \tag{2.24}$$

$$J_{44} = -E\left[\frac{\partial^2 \ln \mathbf{\Lambda}[r_t, \mathbf{\Theta}]}{\partial \alpha_2^2}\right] = \frac{2}{\sigma^2}. \tag{2.25}$$

The off-diagonal elements of the FIM are

$$\begin{aligned} J_{12} &= -E\left[\frac{\partial^2 \ln \mathbf{\Lambda}[r_t, \mathbf{\Theta}]}{\partial \tau_1 \partial \theta_t}\right] \\ &= -\frac{2}{\sigma^2}\Re\left\{\int_0^{T_o} E\left[-\sum_{i=1}^{2}\frac{\partial \tilde{s}_i(t,\mathbf{\Theta})}{\partial \theta_t}\sum_{i=1}^{2}\frac{\partial \tilde{s}_i^*(t,\mathbf{\Theta})}{\partial \tau_1}\right]dt\right\} \\ &\quad -\frac{2}{\sigma^2}\Re\left\{\int_0^{T_o} E\left[\left\{r_t - \sum_{i=1}^{2}\tilde{s}_i(t,\mathbf{\Theta})\right\}\sum_{i=1}^{2}\frac{\partial^2 \tilde{s}_i^*(t,\mathbf{\Theta})}{\partial \theta_t \partial \tau_1}\right]dt\right\}. \end{aligned} \tag{2.26}$$

Since

$$E\left[\left\{r_t - \sum_{i=1}^{2}\tilde{s}_i(t,\mathbf{\Theta})\right\}\sum_{i=1}^{2}\frac{\partial^2 \tilde{s}_i^*(t,\mathbf{\Theta})}{\partial \theta_t \partial \tau_1}\right] = 0,$$

$$J_{12} = \frac{2}{\sigma^2}\Re\left\{\int_0^{T_o}\sum_{i=1}^{2}\frac{\partial \tilde{s}_i(t,\mathbf{\Theta})}{\partial \theta_t}\sum_{i=1}^{2}\frac{\partial \tilde{s}_i^*(t,\mathbf{\Theta})}{\partial \tau_1}dt\right\}. \tag{2.27}$$

More explicitly, J_{12} is found as

$$\begin{aligned} J_{12} =& \frac{2}{\sigma^2}\Re\Bigg\{\tilde{\alpha}_2\tilde{\alpha}_1^* G_2 \int_{-\infty}^{\infty}(2\pi f)^2 e^{-j2\pi f(\tau_2-\tau_1)}|S(f)|^2 df \\ &+ \left[|\tilde{\alpha}_2|^2 G_1 G_2\right]\int_{-\infty}^{\infty}(2\pi f)^2|S(f)|^2 df\Bigg\}. \end{aligned} \tag{2.28}$$

Since the FIM $\mathbf{J}$ is Hermitian symmetric, $J_{21} = J_{12}$.

From Equation 2.4, J_{13} can be written as

$$\begin{aligned} J_{13} &= -E\left[\frac{\partial^2 \ln \mathbf{\Lambda}[r_t, \mathbf{\Theta}]}{\partial\tau_1 \partial\alpha_1}\right] = -E\left[\frac{2}{\sigma^2}\frac{\partial}{\partial\alpha_1}\Re\left\{\int_0^{T_0}\left\{r_t - \sum_{i=1}^{2}\tilde{s}_i(t,\mathbf{\Theta})\right\}\sum_{i=1}^{2}\frac{\partial\tilde{s}_i^*(t,\mathbf{\Theta})}{\partial\tau_1}dt\right\}\right] \\ &= -E\left[\frac{2}{\sigma^2}\Re\left\{\int_0^{T_0}\frac{\partial}{\partial\alpha_1}\left\{r_t - \sum_{i=1}^{2}\tilde{s}_i(t,\mathbf{\Theta})\right\}\sum_{i=1}^{2}\frac{\partial\tilde{s}_i^*(t,\mathbf{\Theta})}{\partial\tau_1}dt\right\}\right] \\ &\quad + E\left[\frac{2}{\sigma^2}\Re\left\{\int_0^{T_0}\left\{r_t - \sum_{i=1}^{2}\tilde{s}_i(t,\mathbf{\Theta})\right\}\sum_{i=1}^{2}\frac{\partial^2\tilde{s}_i^*(t,\mathbf{\Theta})}{\partial\tau_1\partial\alpha_1}dt\right\}\right]. \end{aligned}$$

The second term of the expected value equals to zero and the first term is non-random, thus

$$J_{13} = -E\left[\frac{\partial^2 \ln \mathbf{\Lambda}[r_t, \mathbf{\Theta}]}{\partial\tau_1 \partial\alpha_1}\right] = \frac{2}{\sigma^2}\Re\left\{\int_0^{T_0} e^{j\phi_1}s(t-\tau_1)\sum_{i=1}^{2}\frac{\partial\tilde{s}_i^*(t,\mathbf{\Theta})}{\partial\tau_1}dt\right\}, \tag{2.29}$$

where ϕ_i is the phase of complex ampiltude $\tilde{\alpha}_i$. In similar manner, we obtain J_{14}, J_{23}, J_{24} and J_{34}, respectively, as

$$J_{14} = -E\left[\frac{\partial^2 \ln \mathbf{\Lambda}[r_t, \mathbf{\Theta}]}{\partial\tau_1 \partial\alpha_2}\right] = \frac{2}{\sigma^2}\Re\left\{\int_0^{T_0} e^{j\phi_2}s(t-\tau_2)\sum_{i=1}^{2}\frac{\partial\tilde{s}_i^*(t,\mathbf{\Theta})}{\partial\tau_1}dt\right\} \tag{2.30}$$

$$J_{23} = -E\left[\frac{\partial^2 \ln \mathbf{\Lambda}[r_t, \mathbf{\Theta}]}{\partial\theta_t \partial\alpha_1}\right] = \frac{2}{\sigma^2}\Re\left\{\int_0^{T_0} e^{j\phi_1}s(t-\tau_1)\sum_{i=1}^{2}\frac{\partial\tilde{s}_i^*(t,\mathbf{\Theta})}{\partial\theta_t}dt\right\} \tag{2.31}$$

$$J_{24} = -E\left[\frac{\partial^2 \ln \mathbf{\Lambda}[r_t, \mathbf{\Theta}]}{\partial\theta_t \partial\alpha_2}\right] = \frac{2}{\sigma^2}\Re\left\{\int_0^{T_0} e^{j\phi_2}s(t-\tau_2)\sum_{i=1}^{2}\frac{\partial\tilde{s}_i^*(t,\mathbf{\Theta})}{\partial\theta_t}dt\right\} \tag{2.32}$$

$$J_{34} = -E\left[\frac{\partial^2 \ln \mathbf{\Lambda}[r_t, \mathbf{\Theta}]}{\partial\alpha_1 \partial\alpha_2}\right] = \frac{2}{\sigma^2}\Re\left\{\int_0^{T_0} e^{j(\phi_1-\phi_2)} s(t-\tau_1)s^*(t-\tau_2)dt\right\} \tag{2.33}$$

Through mathematical operations one can write the J_{13}, J_{14}, J_{23}, J_{24} and J_{34} in frequency domain, respectively, as

$$J_{13} = \frac{2}{\sigma^2}\Re\left\{\alpha_1 \int_{-\infty}^{\infty} j2\pi f|S(f)|^2 df + \alpha_2 e^{j(\phi_1-\phi_2)} G_1 \int_{-\infty}^{\infty} j2\pi f e^{-j2\pi f(\tau_1-\tau_2)}|S(f)|^2 df\right\}, \tag{2.34}$$

$$J_{14} = \frac{2}{\sigma^2}\Re\left\{\alpha_2 G_1 \int_{-\infty}^{\infty} j2\pi f|S(f)|^2 df + \alpha_1 e^{j(\phi_2-\phi_1)} \int_{-\infty}^{\infty} j2\pi f e^{j2\pi f(\tau_1-\tau_2)}|S(f)|^2 df\right\}, \tag{2.35}$$

$$J_{23} = \frac{2}{\sigma^2}\Re\left\{\alpha_2 e^{j(\phi_1-\phi_2)} G_2 \int_{-\infty}^{\infty} j2\pi f e^{-j2\pi f(\tau_1-\tau_2)}|S(f)|^2 df\right\}, \tag{2.36}$$

$$J_{24} = \frac{2}{\sigma^2}\Re\left\{\alpha_2 G_2 \int_{-\infty}^{\infty} j2\pi f|S(f)|^2 df\right\}, \tag{2.37}$$

$$J_{34} = \frac{2}{\sigma^2}\Re\left\{e^{j(\phi_1-\phi_2)} \int_{-\infty}^{\infty} e^{-j2\pi f(\tau_1-\tau_2)}|S(f)|^2 df\right\}. \tag{2.38}$$

Since $\mathbf{J}$ is Hermitian symmetric, $J_{ij} = J_{ji}$ so that all the elements of $\mathbf{J}$ are provided.

2.8 Simulations and Discussion

2.8.1 Simulation Results for CRLB

In this section, we provide the simulations results for CRLB for τ_1 and θ_t. The actual parameters are assumed to be $\tau_1 = 2R_d/c$ and $\tau_2 = 2R_{gr}$ where $R_d = 26.92$ m and $R_{gr} = 194.74$ m, $\theta_t = -0.2630$ rad and $\alpha_1 = \alpha_2 = 1$. The radar is located at $h_s = 100$ m above the ground. From our convention, negative θ_t implies that the target is below the radar. These values were chosen such that the multipath is resolvable with the direct path. Using Equation 2.1 the following proves useful in simulating the CRLBS,

$$S(f) \propto \text{sinc}(fT_d), \text{sinc}(x) := \sin(\pi x)/\pi x$$

Our convention is to let the bandwidth refer to $1/T_d$ instead of the classical $2/T_d$. In all the simulations thrice the Nyquist rate was used in simulating the rectangular radar pulses.

In Figure 2, the CRLB on τ_1 is shown when multipath is exploited as well as when it is not, for varying radar bandwidths. In other words, we compare the $CRLB(\tau_1)$ derived here and denoted as $CRLB(\tau_1) - exploited$ to the one derived in (50) but treating τ_2 independent of τ_1 and denoted as $CRLB(\tau_1) - independent$. It is readily seen that through multipath exploitation the CRLB performs much better. For this simulation we choose the noise variance $\sigma^2 = 0.01$ which is 20 dB on both the direct and multipath returns. The bandwidths are chosen starting from 1 MHz to 1000 MHz in multiplicative increments of 10 MHz.

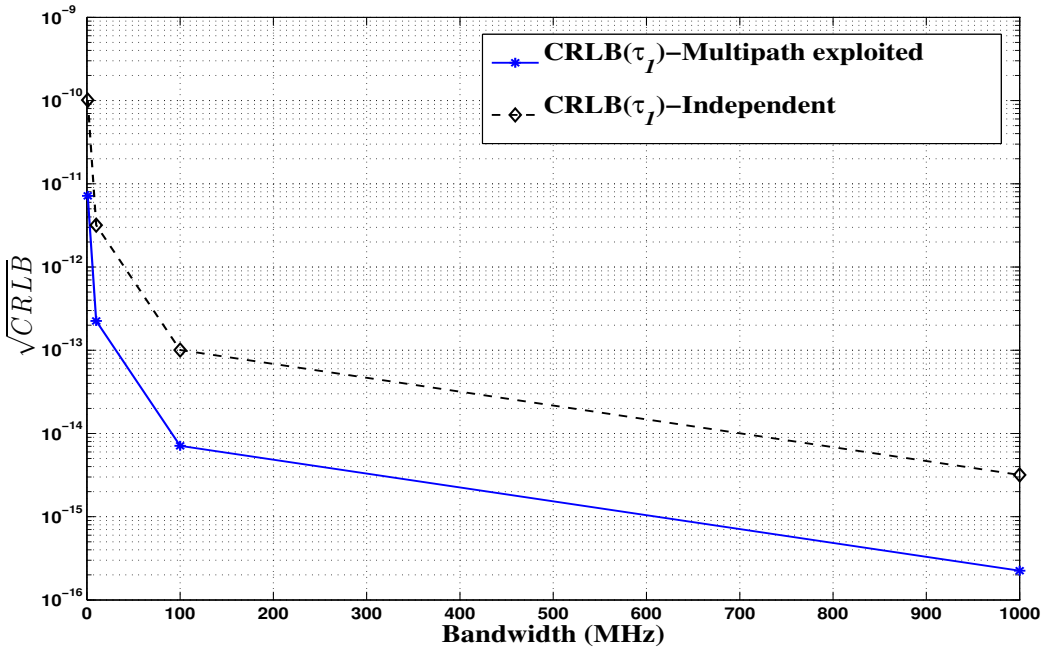

Figure 2. CLRB Comparison: $\hat{\tau}_1$ Multipath Exploited vs Single Path Exploited

In Figure 3 the CRLB is shown for varying bandwidths starting from 1 MHz to 1000 MHz in multiplicative increments of 10 MHz. It is readily seen that the CRLB decreases with increasing bandwidths. For this simulation, the noise variance $\sigma^2 = 1$.

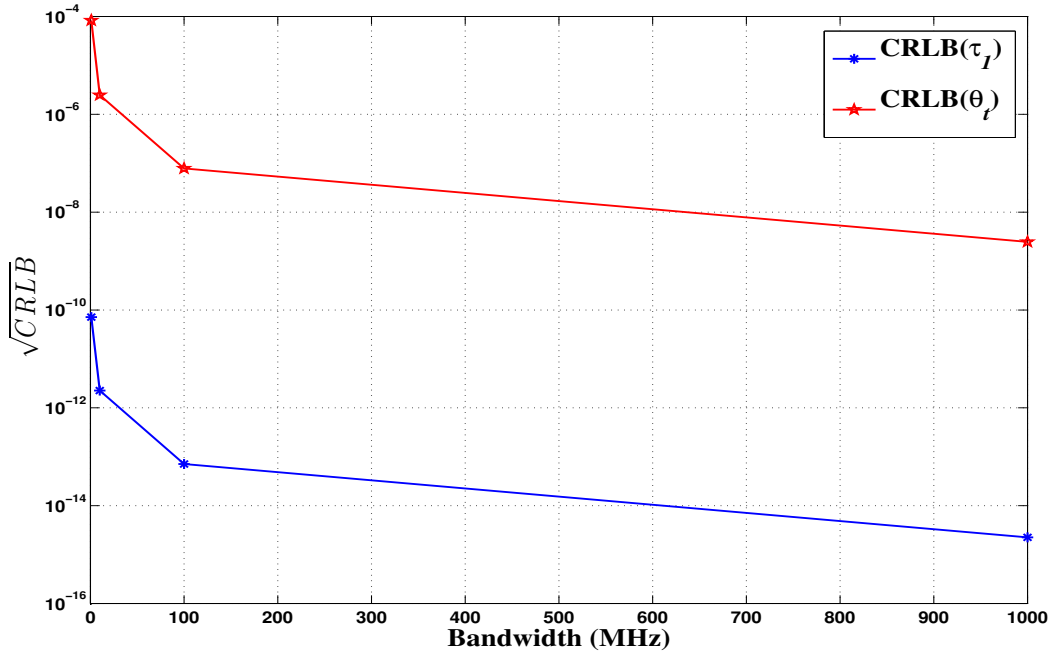

Figure 3. $\tau_{1_{\text{CRLB}}}$ and $\theta_{t_{\text{CRLB}}}$ with respect to Bandwidth

In Figure 4 the CRLB for τ_1 and θ_t are shown for varying noise variance, σ^2. As expected the CRLB increases with increasing σ^2. For this simulation, the bandwidth is 10 MHz.

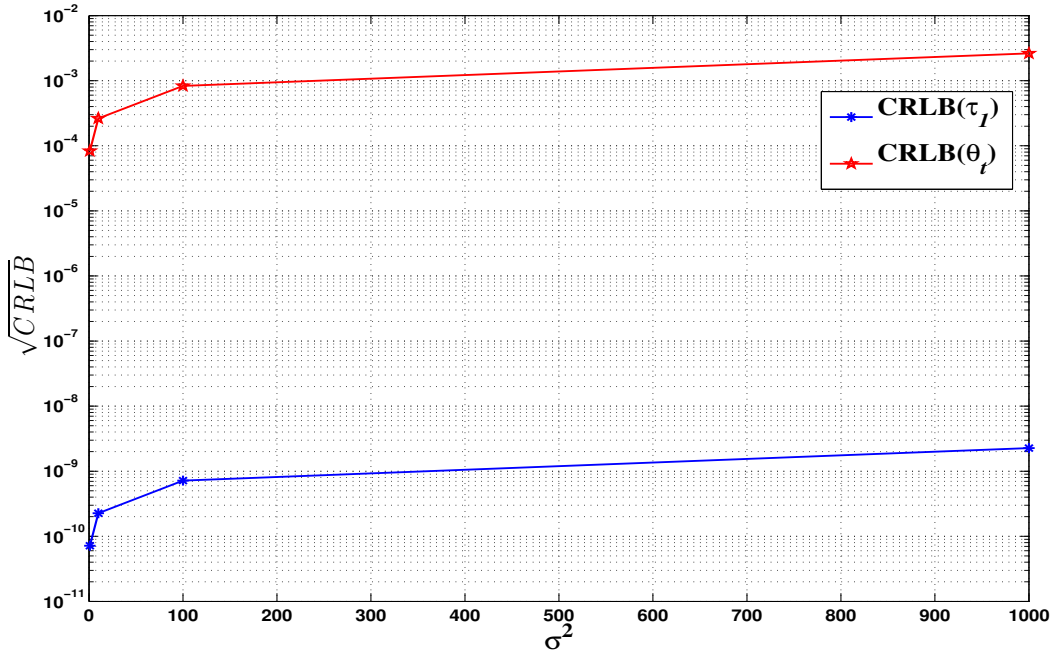

Figure 4. $\tau_{1_{\mathrm{CRLB}}}$ and $\theta_{t_{\mathrm{CRLB}}}$ with respect to σ^2

In Figure 5, the CRLB for α_1 and α_2 are shown for varying noise variance, σ^2. As expected the CRLB increases with increasing σ^2. For this simulation, we assume that $|\alpha 1| = |\alpha_2|$.

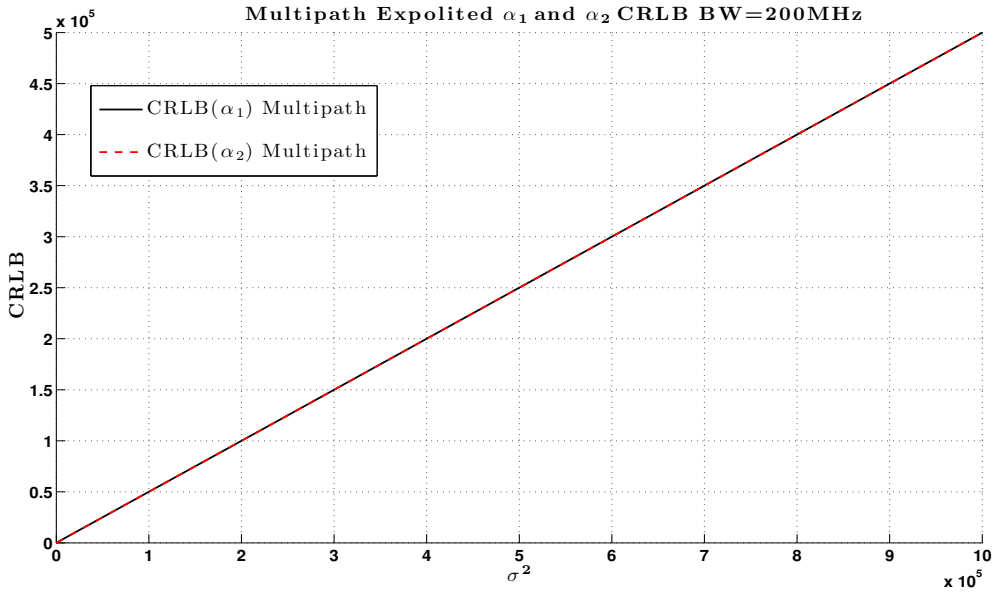

Figure 5. $\alpha_{1_{\text{CRLB}}}$ and $\alpha_{2_{\text{CRLB}}}$ with respect to σ^2

It is well known that the CRLB for time-delay estimation is highly optimistic. Previous studies have shown that the MLE performance for time-delay estimation is much farther away from the CRLB at low SNRs, see for example (53) and references therein. The MLE converges to the CLRB only at reasonable SNRs. This behavior of the MLE for time-delay estimation has prompted the use of other tighter variance bounds such as the Barankin and Ziv-Zakai bounds which have shown to be much tighter than the CRLB. It remains to be seen however, if the

multipath exploited MLE performance is much closer to the multipath exploited CRLB derived here, than their traditional counterpart.

2.8.2 Simulation Results for MLE

In Figure 6 and Figure 7 multipath exploited and single path exploited $\tau_{1_{MSE}}$ and multipath exploited $\hat{\theta}_t$ are presented, respectively, for the BW= 200 MHz and multipath returns are resolvable in time-domain. It is shown that, particularly at higher SNR levels, multipath exploitation is decreasing the mean squared error (MSE) of $\hat{\tau}_1$. MLE is evaluated numerically with Monte Carlo simulation.

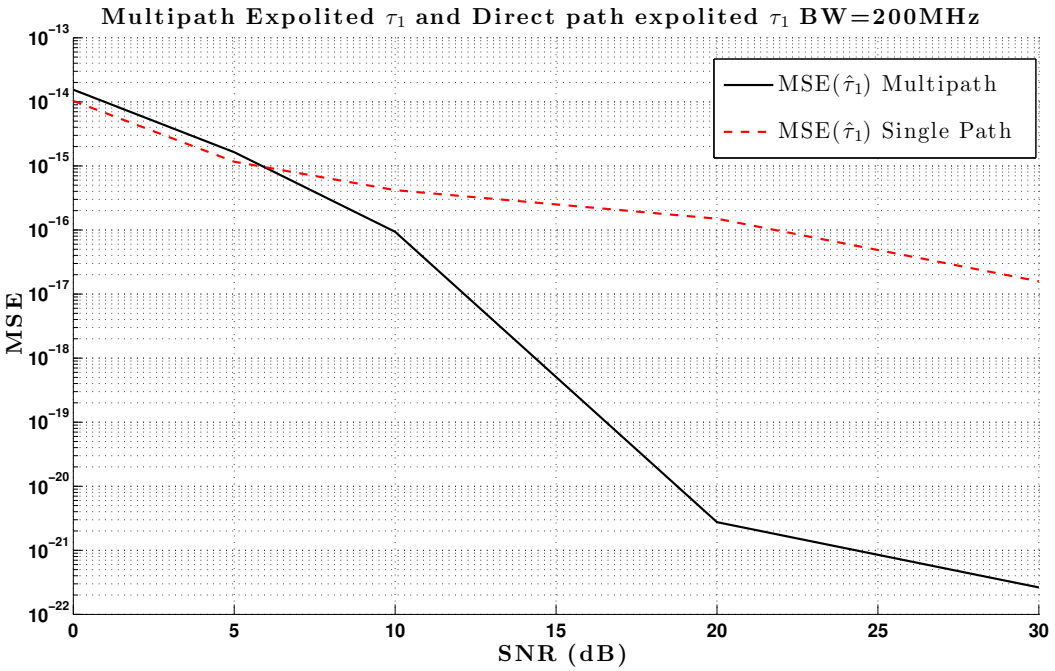

Figure 6. Multipath exploited $\hat{\tau}_{1_{\text{MSE}}}$ and single path exploited $\hat{\tau}_{1_{\text{MSE}}}$ with respect to SNR$= 10\log_{10} 2|\alpha_1|^2/\sigma^2$.

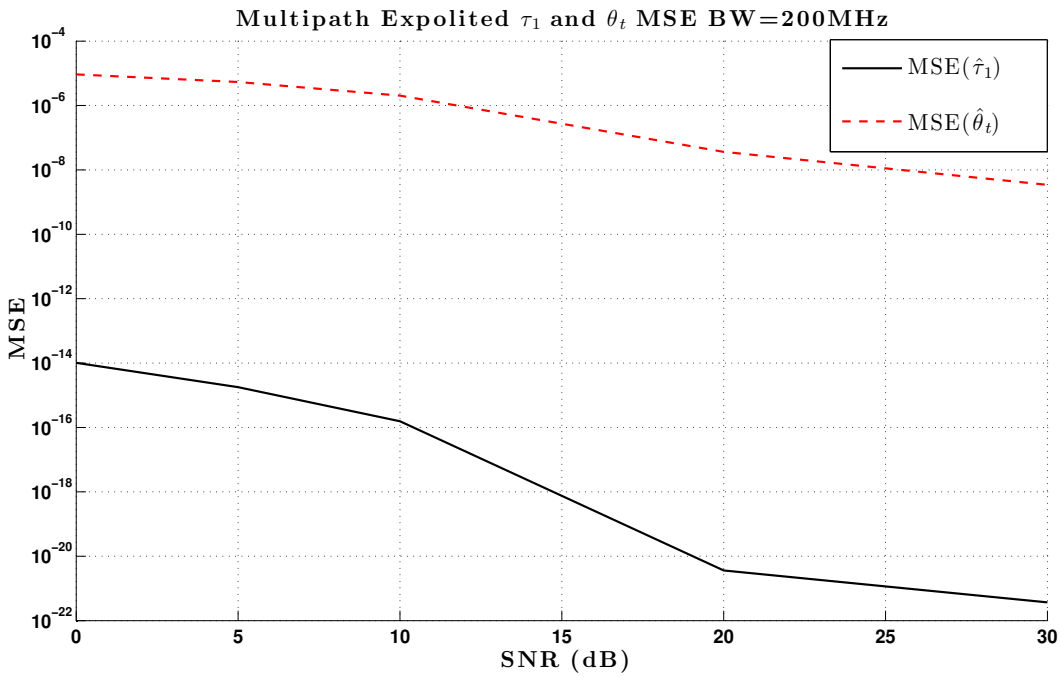

Figure 7. Multipath exploited $\hat{\tau}_{1_{\text{MSE}}}$ and $\hat{\theta}_{t_{\text{MSE}}}$ with respect to SNR$= 10\log_{10} 2|\alpha_1|^2/\sigma^2$.

In Figure 8, the MSE of $\hat{\alpha}_1$ and $\hat{\alpha}_2$ are presented with respect to noise variance σ^2. As expected increasing σ^2 decreases the accuracy of the estimates but more over the MSE increases.

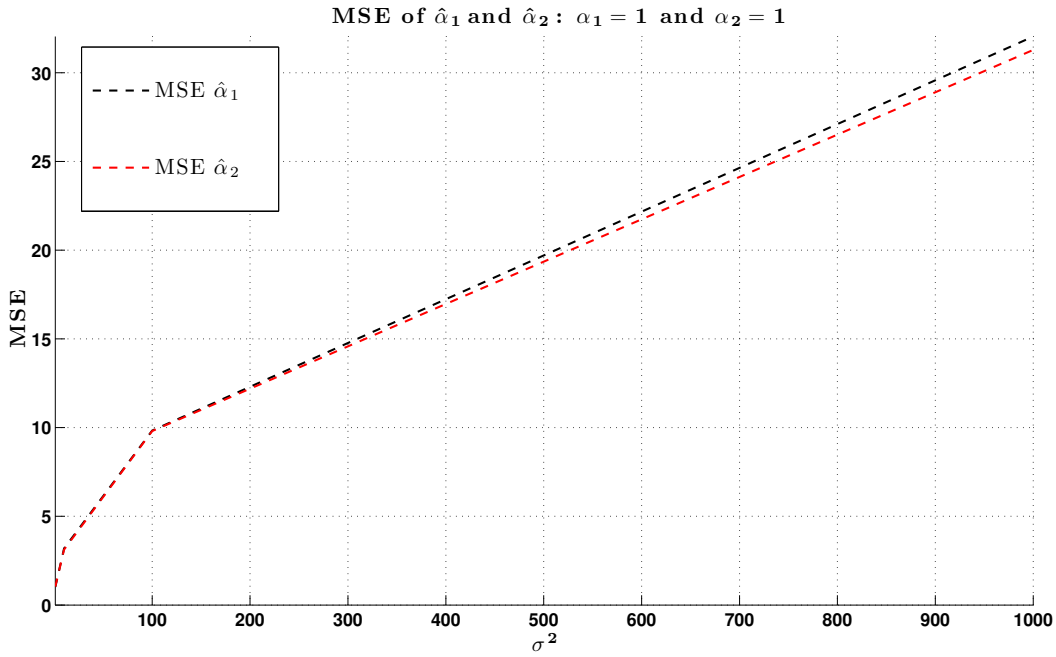

Figure 8. $\alpha_{1_{\text{CRLB}}}$ and $\alpha_{2_{\text{CRLB}}}$ with respect to σ^2

2.9 Conclusion

Maximum likelihood and the Cramér-Rao lower bounds were derived for the multipath exploitation problem. A single wideband radar and a target in a known reflecting geometry were assumed. It was shown here that multipath exploitation offers two advantages, it allows estimation of the AoA and improves the estimation of the direct path time delay in the CRLB sense, which was shown analytically. The former was possible as multipath gave rise to virtual radar sensors, whereas the latter directly followed from parameterizing the multipath time delay as a function of its direct path.

CHAPTER 3

DIVERSE RECEIVING STRATEGIES IN THE PRESENCE OF MULTIPATH WITH PRIOR KNOWLEDGE OF THE ENVIRONMENT

3.1 Introduction

This chapter is focused on improving the probability of detection of a radar target by taking advantage of prior knowledge of the radar-target environment and devising appropriate detectors based upon the region where the target is located. The improvement is computed with respect to a conventional detection problem based on a model of the return signal that accounts only for the direct signal from the target.

Radar detection problems are still challenging in all environments where multipath effects are present, notwithstanding the fact that they have been widely studied through advanced electromagnetic modeling (1), (2). One approach to deal with multipath problems is to take the advantage of diversity (3). In addition, with adaptive radars, prior knowledge about the environment and its effective parameters enhance the detection performance of radar systems (4)-(11).

This chapter is organized as in the following. First, we consider a basic case study to show how to conduct an electromagnetic analysis that takes advantage of prior knowledge of the environment where the radar operates. As a result, we obtain the propagation time of each multipath component. Then, the propagation time information is used to partition

the environment into regions where diverse receiving strategies are applied. The criterion to determine the regions is the amount of overlap, in the time-domain, of the multipath components of the received signal. The amount of overlap depends on the environment, the location of radar and target, and the duration of the transmitted pulse. Accordingly, the general received signal model is specialized within each region to account for the presence of significant overlap or its absence. Then, within each region, a different receiver is devised thus justifying the statement of diverse receiving strategies. Neyman-Pearson tests (NP) as optimum detectors, and Generalized Likelihood Ratio Tests (GLRT) as sub-optimum detectors are devised for each region. Finally, the performance of two detection strategies based on two distinct multipath structures of a radar-target environment is presented under the assumption of a zero-mean complex circular Gaussian noise (CWGN) with known power spectral density (PSD) σ^2. One strategy, associated with NP1 and GLRT1 receivers is considered for highly clumped multipath returns in the time-domain, while the other strategy, associated with NP2 and GLRT2 receivers, which are exploiting multipath in the target detection, is taken for entirely resolvable multipath returns in time-domain. The performance comparison is conducted also particularly in a transition region, where multipath components are neither entirely resolvable nor highly clumped in time-domain. A qualitative analysis of the improvement in the target probability of detection with multipath exploitation is provided.

There are two main contributions in this chapter. First, it is possible to improve the probability of detection when the multipath components are distinguishable, compared to a conventional detector that does not take multipath information into account. A qualitative

analysis is provided for the improvement in the target probability of detection via multipath exploitation when the multipath components are distinguishable and partially overlap in the time-domain. Second, it is possible to design detectors that have the best performance based upon *a-priori* knowledge of the region where the target is located.

Preliminary results were presented in (36)-(40).

3.2 Multipath Model and Time-Delay Analysis

3.2.1 Multipath Propagation Model

The geometry of the basic radar-target environment, which causes multipath propagation, is illustrated in Figure 9. We focus on a propagation model that contains only a few parameters to describe the environment, so as to enable an analytic discussion of the detection problem. In Figure 9, the origin of the cartesian coordinate system is the location of the radar and the target is located in a vertical plane at (x_t, z_t) so that we investigate a 2-D geometry.

A high frequency ray-tracing electromagnetic analysis of this geometry leads to a propagation model consisting of two rays, with propagation times τ_1 and τ_2, and provides the following expression for the received signal of interest

$$\tilde{r}_s(t) = \tilde{\alpha}_1(t)s(t-\tau_1) + \tilde{\alpha}_2(t)s(t-\tau_2), \tag{3.1}$$

where $\tilde{r}_s(t)$ and $s(t)$ are the baseband equivalents of the received signal of interest and transmitted signal respectively, $\tilde{\alpha}_1(t)$ and $\tilde{\alpha}_2(t)$ are the complex unknown deterministic parameters

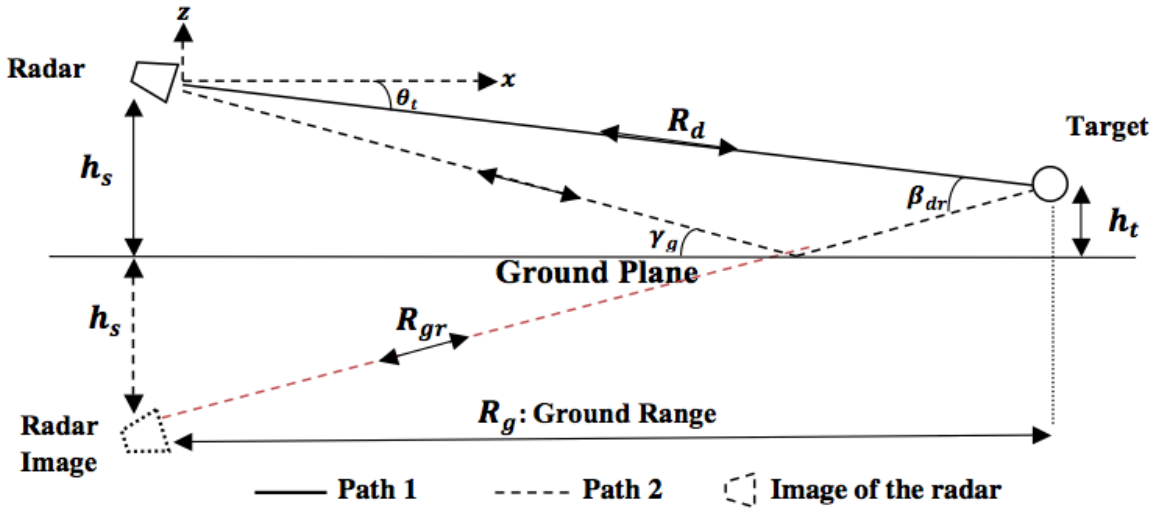

Figure 9. Geometry of the problem: Radar-Target over a Ground Plane.

accounting for propagation and scattering effects, and τ_1 and τ_2 are the time delays along the corresponding propagation paths.

The electromagnetic ray-tracing analysis of the environment is always capable to predict the time-delays associated with each multipath component as shown, for example, in (41), (42), (49).

3.2.2 Time-Delay Analysis Based on Target Location

In order to conduct a time-delay analysis over the region of interest, we compute time-delays and associated time-delay differences for all hypothetical locations of the target. In Figure 9, we have the following parameters:

- R_d: Radial range between radar and target

- R_g: Ground range between radar and target
- R_{gr}: Radial range between image of the radar and the target (or between the radar and image of the target)
- h_s: Radar height above ground surface
- h_t: Target height above ground surface
- θ_t: Elevation angle between radar and target
- γ_g: Grazing angle with ground surface
- β_{dr}: Bistatic angle at target position between radar and its image.

Then, the time-delays and associated time-delay difference for all possible locations of the target are, (36), (37),

$$\tau_1 = \frac{2R_d}{c} = \frac{2}{c}\sqrt{x_t^2 + z_t^2}, \tag{3.2}$$

$$\tau_2 = \frac{2R_{gr}}{c} = \frac{2}{c}\sqrt{x_t^2 + (h_t + h_s)^2}, \tag{3.3}$$

$$|\tau_2 - \tau_1| = \frac{2}{c}\left|\sqrt{x_t^2 + (h_s + h_t)^2} - \sqrt{x_t^2 + z_t^2}\right|. \tag{3.4}$$

Based on Equation 3.2-Equation 3.4, we construct a map showing the value of $|\tau_2 - \tau_1|$ for all hypothetical target locations in the region of interest, as shown in Figure 10, to provide an understanding of how $|\tau_2 - \tau_1|$ behaves at each range-cell for a given transmitted pulse duration $T = 10$ ns.

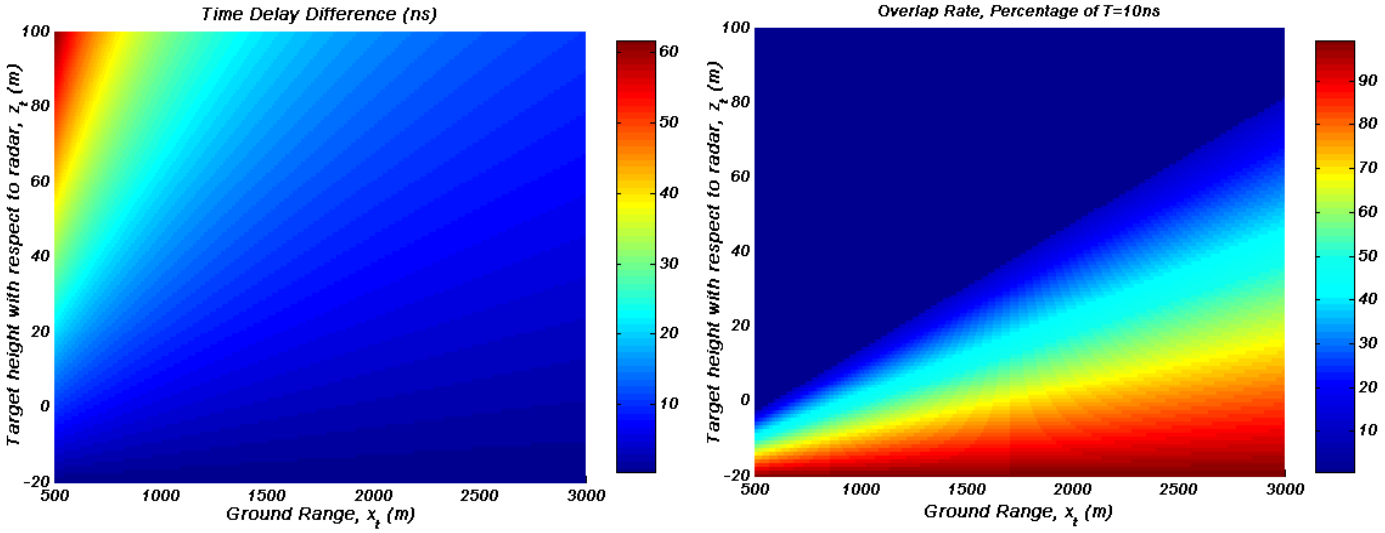

(a) Time-Delay Difference

(b) Overlap Rate

Figure 10. Time-Delay Mapping Based on Target Location

Additionally, for a given T, we obtain the sub-regions where multipath signal components overlap, when $|\tau_2 - \tau_1| \leq T$, and those where the multipaths are distinguishable, when $|\tau_2 - \tau_1| > T$. This is shown in Figure 11, when $T = 10$ ns, and it prompts us to diversify the detection strategy within each region.

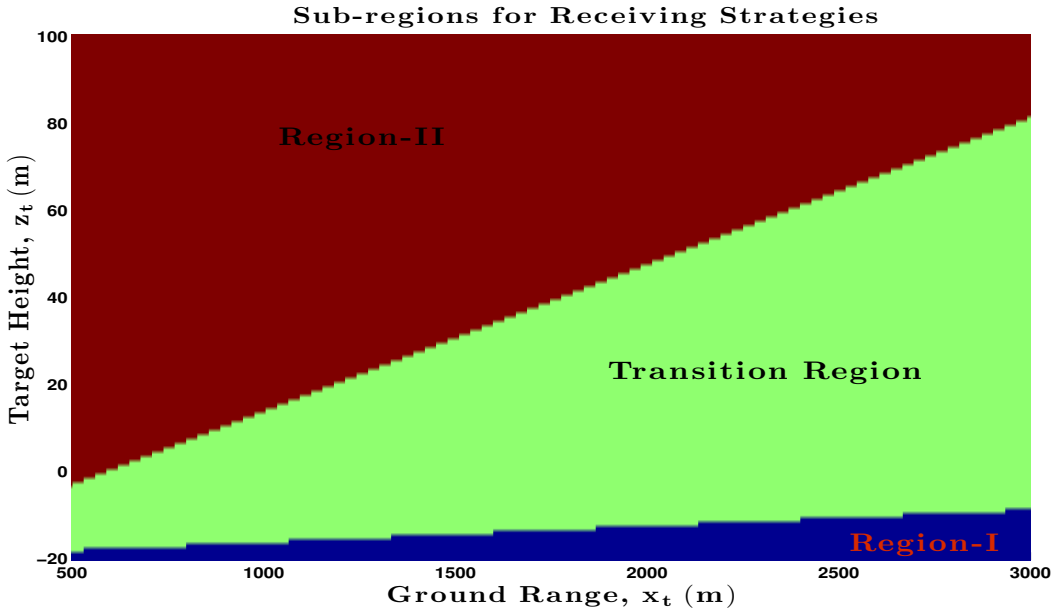

Figure 11. Sub-regions for Receiving Strategies
(i) Region-I: Multipath returns are highly clumped; (ii) Region-II: Multipath returns are entirely resolvable; and, (iii) Transition region: Mutlipath returns are neither highly clumped nor resolvable in time-domain.

3.3 Formulation of the Detection Problem

The signal representations and corresponding hypothesis testing problems for each region are derived. Exploiting the useful received signal model given in Equation 3.1, we assume

$$s(t) = \begin{cases} \frac{1}{\sqrt{T}} & 0 \le t \le T \\ 0 & \text{elsewhere} \end{cases}, \tag{3.5}$$

$$\tilde{\alpha}_1(t) = \begin{cases} \text{unknown} & \tau_1 \le t \le T + \tau_1 \\ 0 & \text{elsewhere} \end{cases}, \tag{3.6}$$

$$\tilde{\alpha}_2(t) = \begin{cases} \text{unknown} & \tau_2 \le t \le T + \tau_2 \\ 0 & \text{elsewhere} \end{cases}. \tag{3.7}$$

The pulse duration T is assumed to be small compared to the coherence time of the target, so that $\tilde{\alpha}_1(t)$ and $\tilde{\alpha}_2(t)$ can be approximated with two unknown deterministic constants $\tilde{\alpha}_1$ and $\tilde{\alpha}_2$, respectively.

Region-I is defined by $|\tau_2 - \tau_1| \ll T$ and the received signal (under the hypothesis where target is present) is represented as

$$\begin{aligned} \tilde{r}(t) &= \tilde{\alpha}_1 s(t-\tau_1) + \tilde{\alpha}_2 s(t-\tau_2) + \tilde{w}(t) \\ &\simeq \tilde{\alpha} s(t-\tau_1) + \tilde{w}(t) \end{aligned} \tag{3.8}$$

without any significant loss of the received energy. $\tilde{\alpha}$ is an unknown complex deterministic parameter, $\tilde{r}(t)$ and $\tilde{w}(t)$ are the baseband equivalents of the received signal and noise, respectively. Accordingly, the detection problem can be formulated as the following hypothesis test

$$\begin{aligned} H_0: &\quad \tilde{r}(t) = \tilde{w}(t) \\ H_1: &\quad \tilde{r}(t) = \tilde{\alpha} s(t-\tau_1) + \tilde{w}(t) \end{aligned} \qquad t \in [\tau_1, T+\tau_1] \tag{3.9}$$

where $[\tau_1, T+\tau_1]$ is the observation interval.

Region-II is defined by $|\tau_2 - \tau_1| \geq T$; hence multipath components are resolvable in time-domain and exploited in the receiver. Accordingly, the detection problem can be formulated as

$$\begin{aligned} H_0: &\quad \tilde{r}(t) = \tilde{w}(t) \\ H_1: &\quad \tilde{r}(t) = \tilde{\alpha}_1 s(t-\tau_1) + \tilde{\alpha}_2 s(t-\tau_2) + \tilde{w}(t) \end{aligned} \tag{3.10}$$

where $t \in [\tau_1,\ T+\tau_2]$, which is the observation interval. Since $|\tau_2 - \ \tau_1| \geq \ T,\ \ s(t-\tau_1)$ and $s(t-\tau_2)$ are orthogonal signals, namely we have $\int_{-\infty}^{\infty} s(t-\tau_1)\ s^*(t-\tau_2)\ dt = 0$, where $(.)^*$ is the complex conjugate operator.

The likelihood ratio test in both regions can be written as

$$\Lambda[\tilde{r}(t)|\boldsymbol{\Theta}] = \frac{p_{\tilde{r}(t)|\boldsymbol{\Theta},H_1}\left(\tilde{r}(t)|\boldsymbol{\Theta},H_1\right)}{p_{\tilde{r}(t)|H_0}\left(\tilde{r}(t)|H_0\right)}, \tag{3.11}$$

where $p_{\tilde{r}(t)|\boldsymbol{\Theta},H_1}\left(\tilde{r}(t)|\boldsymbol{\Theta},H_1\right)$ and $p_{\tilde{r}(t)|H_0}\left(\tilde{r}(t)|H_0\right)$ are the likelihood functions, $\boldsymbol{\Theta}$ is the vector of unknown parameters, *i.e.*

$$\boldsymbol{\Theta} = \begin{cases} [\tilde{\alpha}] & \text{in Region-I} \\ [\tilde{\alpha}_1, \tilde{\alpha}_2]^T & \text{in Region-II.} \end{cases} \tag{3.12}$$

In the Transition Region, the time-delay difference is shorter than the transmitted pulse duration T but not as short as in region-I, *i.e* $|\tau_2 - \tau_1| < T$. Thus multipath return signals along different paths are neither highly clumped nor resolvable in time-domain. The received signal in the Transition Region under the hypotheses H_0 and H_1 are the same as Equation 3.10

in region-II. However, $s(t-\tau_1)$ and $s(t-\tau_2)$ are no longer orthogonal signals since $|\tau_2 - \tau_1| < T$ and we have $\int_{-\infty}^{\infty} s(t-\tau_1)\ s^*(t-\tau_2)\ dt = \rho$, which is a real number in this particular scenario.

3.4 Optimum and Sub-Optimum Detectors

The optimum and sub-optimum detectors are sought assuming that $\tilde{w}(t)$ is a zero-mean complex circular white Gaussian noise (CWGN), with known power spectral density (PSD) σ^2. A conventional approach is adopted based on projecting the received waveform along the first M functions of an orthonormal basis and letting M diverge. Precisely, having chosen the basis ß $= \{\phi_i(t)\}_{i=1}^{\infty}$, the received signal is represented by components $R_i = \langle \tilde{r}(t), \phi_i(t) \rangle$, where $\langle \cdot, \cdot \rangle$ denotes the scalar product in the space of finite energy signals. Then the likelihood ratio Equation 3.11 can be written as

$$\begin{aligned} \Lambda[\tilde{r}(t)|\mathbf{\Theta}] &= \lim_{M\to\infty} \Lambda_M[r_M(t)|\mathbf{\Theta}] \\ &= \lim_{M\to\infty} \frac{p_{\mathbf{R_M}|\mathbf{\Theta},H_1}\left(\mathbf{R_M}|\mathbf{\Theta}, H_1\right)}{p_{\mathbf{R_M}|H_0}\left(\mathbf{R_M}|H_0\right)}, \end{aligned} \tag{3.13}$$

where $\mathbf{R_M}$ is the vector containing the first M coefficients of the received signal waveform and $r_M(t)$ is the projection of the received signal on the subspace spanned by the first M functions of the basis, (44), (51). Since we have zero mean CWGN with PSD σ^2, R_i is complex Gaussian with (i) μ_i mean and variance σ^2 under H_1 hypothesis; and (ii) zero mean and variance σ^2 under H_0 hypothesis. Thus, the likelihood function is readily found as

$$\lim_{M\to\infty} \Lambda_M[r_M(t)|\mathbf{\Theta}] = \lim_{M\to\infty} \frac{\prod_{i=1}^{M} \frac{1}{\pi\sigma^2} \exp\left(-\frac{|R_i-\mu_i|^2}{\sigma^2}\right)}{\prod_{i=1}^{M} \frac{1}{\pi\sigma^2} \exp\left(-\frac{|R_i|^2}{\sigma^2}\right)}, \tag{3.14}$$

where μ_i is the expected value of R_i.

First we assume that $\boldsymbol{\Theta}$ is a known set of parameters in order to deduct the optimal detector. Although this hypothesis is not realistic for real world radar and sonar problems, it provides an upper bound for any receiver operating under the same signal model. It is also important to observe whether a Uniformly Most Powerful (UMP) test exists or does not exist.

3.4.1 Region-I: Multipath returns are highly clumped

We formulate the detection problem, based on Equation 3.9, as

$$\begin{aligned} H_1\text{:}\quad & R_i = \langle \tilde{r}(t), \phi_i(t) \rangle = \begin{cases} \tilde{\alpha} + \tilde{w}(1), & i = 1 \\ \tilde{w}(i), & i > 1 \end{cases} \\ H_0\text{:}\quad & R_i = \langle \tilde{r}(t), \phi_i(t) \rangle = \tilde{w}(i) \end{aligned} \tag{3.15}$$

where $\phi_1(t) = s(t - \tau_1)$, so that $\mu_1 = \tilde{\alpha}$ and $\mu_{i \neq 1} = 0$. By evaluating the likelihood ratio Equation 3.14 with the knowledge of $\boldsymbol{\Theta}$ and taking the logarithm, one obtains the log-likelihood ratio, up to a constant and irrelevant factor, as

$$\ln \Lambda[\tilde{r}(t)|\boldsymbol{\Theta}] = \frac{|R_1|^2 - |R_1 - \tilde{\alpha}|^2}{\sigma^2}. \tag{3.16}$$

Then the corresponding NP test, which we call NP1, is given as, (51; 46),

$$\Re \left\{ \sqrt{\frac{2}{\sigma^2}} \tilde{\alpha}^* R_1 \right\} \underset{H_0}{\overset{H_1}{\gtrless}} \gamma_1, \tag{3.17}$$

where $\Re\{.\}$ is the real part operator and γ_1 is the threshold. This is a hypothetical test with the perfect measurement or the knowledge of $\tilde{\alpha}$ in the detector. Although Equation 3.17 is not a UMP test with respect to $\tilde{\alpha}$, it provides an upper bound to the performance of any practically implementable detector. GLRT is a common technique to devise detectors with unknown parameters, particularly when no UMP test exists. GLRT uses the maximum likelihood estimates (MLE) of unknown parameters under both hypotheses in the likelihood ratio (51), (46).

Thus, the corresponding GLRT detector with respect to $\tilde{\alpha}$ is given as

$$\frac{2}{\sigma^2}|R_1|^2 \underset{H_0}{\overset{H_1}{\gtrless}} \gamma_1', \tag{3.18}$$

which we call GLRT1. It can be realized with a standard matched-filter followed by square modulus (51), (46).

3.4.2 Region-II: Multipath returns are entirely resolvable

The basis functions $ß = \{\phi_i(t)\}_{i=1}^{M}$ are selected as

$$\begin{aligned} \phi_1(t) &= s(t-\tau_1) \quad \tau_1 \le t \le T+\tau_1 \\ \phi_2(t) &= s(t-\tau_2) \quad \tau_2 \le t \le T+\tau_2 \end{aligned} \tag{3.19}$$

so that the detection problem for region-II becomes

$$\begin{aligned} H_1\text{:}\quad R_i &= \langle \tilde{r}(t), \phi_i(t) \rangle = \begin{cases} \tilde{\alpha}_1 + \tilde{w}(1), & i = 1 \\ \tilde{\alpha}_2 + \tilde{w}(2), & i = 2 \\ \tilde{w}(i), & i > 2 \end{cases} \\ H_0\text{:}\quad R_i &= \langle \tilde{r}(t), \phi_i(t) \rangle = \tilde{w}(i). \end{aligned} \tag{3.20}$$

By evaluating the likelihood ratio Equation 3.14 in region-II with the knowledge of $\mathbf{\Theta}$ and taking the logarithm, we obtain the corresponding log-likelihood ratio, up to a constant and irrelevant factor, as

$$\ln \Lambda[\tilde{r}(t)|\mathbf{\Theta}] = -\frac{|R_1 - \tilde{\alpha}_1|^2 + |R_2 - \tilde{\alpha}_2|^2}{\sigma^2} + \frac{|R_1|^2 + |R_1|^2}{\sigma^2}. \tag{3.21}$$

After simple manipulations, the log-likelihood ratio test, which we call NP2, is derived as

$$\Re\left\{ \sqrt{\frac{2}{\sigma^2}} \left[\tilde{\alpha}_1^* R_1 + \tilde{\alpha}_2^* R_2 \right] \right\} \underset{H_0}{\overset{H_1}{\gtrless}} \gamma_2, \tag{3.22}$$

where γ_2 is the threshold. This is a hypothetical test with the perfect measurement or the knowledge of $\tilde{\alpha}_1$ and $\tilde{\alpha}_2$ in the detector. Additionally, it is not a UMP test with respect to $\tilde{\alpha}_1$ and $\tilde{\alpha}_2$, thus GLRT approach is applied next.

GLRT substitutes the unknown signal parameters with $\hat{\mathbf{\Theta}} = [\hat{\tilde{\alpha}}_1, \hat{\tilde{\alpha}}_2]^T$ in the log-likelihood ratio Equation 3.21. $\hat{\mathbf{\Theta}}$ is the MLE of $\mathbf{\Theta}$ under H_1 that maximizes the corresponding likelihood function, (38) and (46), *i.e.*

$$\hat{\mathbf{\Theta}} = [\hat{\tilde{\alpha}}_1, \hat{\tilde{\alpha}}_2]^T = [R_1, R_2]^T. \tag{3.23}$$

The corresponding GLRT, which we call GLRT2, can be written as

$$\frac{2}{\sigma^2}\left[|R_1|^2 + |R_2|^2\right] \underset{H_0}{\overset{H_1}{\gtrless}} \gamma_2'. \tag{3.24}$$

3.4.3 Transition Region

In the Transition Region, *i.e.* $|\tau_2 - \tau_1| < T$, no particular detector is devised since there is no stable structure of multipath returns, *i.e.* $\int_{-\infty}^{\infty} s(t-\tau_1)s^*(t-\tau_2)dt = \rho$ where $\rho \in [-1, 1]$. Rather, we analyze the performance of NP2 and GLRT2, which exploits multipath, in comparison with NP1 and GLRT1, respectively, which exploits the direct path return only.

3.5 Performance Assessment

In this section, we assess the performance of the proposed detectors GLRT2 Equation 3.24 and NP2 Equation 3.22, which exploit multipath, as well as the conventional detectors GLRT1 Equation 3.18 and NP1 Equation 3.17, which only account for the direct return signals.

Before discussing the performance of these detectors, we need to define the corresponding probabilities of false alarm and detection.

3.5.1 Probabilities of False Alarm and Detection

The probability of false alarm of NP1 is

$$P_{FA_{\mathbf{NP1}}} = Q\left(\frac{\gamma_1}{\sqrt{|\tilde{\alpha}|^2}}\right) \tag{3.25}$$

yielding the threshold,

$$\gamma_1 = |\tilde{\alpha}| Q^{-1}\left(P_{FA_{\mathbf{NP1}}}\right) \tag{3.26}$$

and the corresponding probability of detection,

$$P_{D_{\mathbf{NP1}}} = Q\left(Q^{-1}(P_{FA_{\mathbf{NP1}}}) - \sqrt{\frac{|\tilde{\alpha}|^2}{\sigma^2/2}}\right), \tag{3.27}$$

where $Q(.)$ and $Q^{-1}(.)$ are the Complementary Cumulative Distribution Function (CCDF), and inverse CCDF of a standard Gaussian random variable, respectively, (46). The probability of false alarm of GLRT1 is

$$P_{FA_{\mathbf{GLRT1}}} = Q_{\chi_2^2}\left(\gamma_1'\right) \tag{3.28}$$

yielding the threshold

$$\gamma_1' = Q_{\chi_2^2}^{-1}\left(P_{FA_{\mathbf{GLRT1}}}\right) \tag{3.29}$$

and the corresponding probability of detection,

$$P_{D_{\mathbf{GLRT1}}} = Q_{\chi_2'^2(\lambda)}\left(Q_{\chi_2^2}^{-1}\left(P_{FA_{\mathbf{GLRT1}}}\right)\right), \tag{3.30}$$

where $Q_{\chi_2^2}(.)$ and $Q_{\chi_2'^2(\lambda)}(.)$ are the CCDF of a χ_2^2, and a $\chi_2'^2(\lambda)$ where non-centrality parameter $\lambda = 2|\tilde{\alpha}|^2/\sigma^2$, respectively, (46).

The test statistics of NP2 under both hypotheses are Gaussian, thus the probability of false alarm is obtained as

$$P_{FA_{\mathbf{NP2}}} = Q\left(\frac{\gamma_2}{\sqrt{(|\tilde{\alpha}_1|^2 + |\tilde{\alpha}_2|^2)}}\right) \tag{3.31}$$

yielding the threshold,

$$\gamma_2 = Q^{-1}(P_{FA})\sqrt{|\tilde{\alpha}_1|^2 + |\tilde{\alpha}_2|^2} \tag{3.32}$$

and the probability of detection,

$$P_{D_{\mathbf{NP2}}} = Q\left(Q^{-1}(P_{FA_{\mathbf{NP2}}}) - \sqrt{\frac{|\tilde{\alpha}_1|^2 + |\tilde{\alpha}_2|^2}{\sigma^2/2}}\right). \tag{3.33}$$

When we consider GLRT2 under H_0, the test statistics is the product between $2/\sigma^2$ and the sum of the square magnitudes of two complex circular Gaussian variables with zero mean

and variance σ^2. It can be shown that this test statistics has χ^2_4 distribution. Consequently, the probability of false alarm can be written as

$$P_{FA_{\mathbf{GLRT2}}} = Q_{\chi^2_4}\left(\gamma_2'\right) \tag{3.34}$$

yielding the threshold,

$$\gamma_2' = Q^{-1}_{\chi^2_4}\left(P_{FA_{\mathbf{GLRT2}}}\right). \tag{3.35}$$

However, when we consider GLRT2 under H_1, the test statistics is the product between $2/\sigma^2$ and the sum of the square magnitudes of two complex circular Gaussian random variables with non-zero mean and variance σ^2. Again, it can be shown that the test statistics has a $\chi'^2_4(\lambda_{12})$ distribution, (52). As a consequence, the probability of detection of GLRT2 can be written as

$$P_{D_{\mathbf{GLRT2}}} = Q_{\chi'^2_4(\lambda_{12})}\left(Q^{-1}_{\chi^2_4}\left(P_{FA_{\mathbf{GLRT2}}}\right)\right) \tag{3.36}$$

where

$$\lambda_{12} = \frac{2}{\sigma^2}(|\tilde{\alpha}_1|^2 + |\tilde{\alpha}_2|^2) = \lambda_1 + \lambda_2 \tag{3.37}$$

where $\lambda_1 = 2|\tilde{\alpha}_1|^2/\sigma^2$ and $\lambda_2 = 2|\tilde{\alpha}_2|^2/\sigma^2$. It is also important to note that $\lambda = \lambda_1$, *i.e.* $\tilde{\alpha} = \tilde{\alpha}_1$, in Region-II.

In the Transition Region no new detectors are devised, but rather we explore the use of GLRT1 and GLRT2. Accordingly, we first determine their statistical characterizations. Then the corresponding probabilities of false alarm and detection are provided.

The probabilities of false alarm of NP1 and GLRT1 in the Transition Region are the same as Equation 3.25 and Equation 3.28, respectively, but the probabilities of detection change and are obtained as

$$P_{D_{NP1_T}} = Q\left(Q^{-1}\left(P_{FA_{NP1}}\right) - \frac{|\tilde{\alpha}_1|^2 + \Re\{\rho\tilde{\alpha}_1^*\tilde{\alpha}_2\}}{\sqrt{|\tilde{\alpha}_1|^2\sigma^2/2}}\right) \tag{3.38}$$

and

$$P_{D_{\mathbf{GLRT1_T}}} = Q_{\chi_2'^2(\lambda_T)}\left(Q_{\chi_2^2}^{-1}\left(P_{FA_{\mathbf{GLRT1}}}\right)\right) \tag{3.39}$$

where

$$\lambda_T = \frac{2}{\sigma^2}|\tilde{\alpha}_1 + \rho\tilde{\alpha}_2|^2. \tag{3.40}$$

Based on the received signal definition in Equation 3.10 and the test statistics of the NP2 Equation 3.22 and GLRT2 Equation 3.24, the probabilities of false alarm and detection in the Transition Region are not the same as Equation 3.31, Equation 3.33, Equation 3.34 and Equation 3.36, respectively. The covariance of the random variables R_1 and R_2 in detectors has

to be taken into account to characterize the probability distribution functions. The covariance of R_1 and R_2 is readily found by $COV\left[R_1, R_2^*\right] = \rho\sigma^2$.

The probabilities of false alarm and detection of NP2 are obtained respectively as

$$P_{FA_{\mathbf{NP2_T}}} = Q\left(\frac{\gamma_2}{\sqrt{|\tilde{\alpha}_1|^2 + |\tilde{\alpha}_2|^2 + 2\rho\Re\{\tilde{\alpha}_1\tilde{\alpha}_2^*\}}}\right), \tag{3.41}$$

$$P_{D_{\mathbf{NP2_T}}} = Q\left(Q^{-1}(P_{FA_{\mathbf{NP2_T}}}) - \sqrt{\frac{|\tilde{\alpha}_1|^2 + |\tilde{\alpha}_2|^2 + 2\rho\Re\{\tilde{\alpha}_1\tilde{\alpha}_2^*\}}{\sigma^2/2}}\right). \tag{3.42}$$

The test statistics of GLRT2 is the sum of square magnitudes of two correlated complex circular Gaussian random variables R_1 and R_2 with the covariance matrix $\mathbf{C_R}$, where

$$\mathbf{C_R} = \sigma^2 \begin{bmatrix} 1 & \rho \\ \rho & 1 \end{bmatrix}, \tag{3.43}$$

by letting $\mathbf{R} = [R_1, R_2]^T$. We represent Equation 3.24 in the Transition Region with two statistically independent random variables, obtaining

$$[(1+\rho)R_s + (1-\rho)R_d] \underset{H_0}{\overset{H_1}{\gtrless}} \gamma_2', \tag{3.44}$$

where $R_s = \frac{|R_1+R_2|^2}{\sigma^2(1+\rho)}$, and $R_d = \frac{|R_1-R_2|^2}{\sigma^2(1-\rho)}$. They are two independent random variables that have χ_2^2 distribution under H_0, $\chi_2'^2(\lambda_s)$ and $\chi_2'^2(\lambda_d)$ distributions, respectively, under H_1, where

$$\lambda_s = \frac{(1+\rho)|\tilde{\alpha}_1 + \tilde{\alpha}_2|^2}{\sigma^2} \tag{3.45}$$

$$\lambda_d = \frac{(1-\rho)|\tilde{\alpha}_1 - \tilde{\alpha}_2|^2}{\sigma^2} \tag{3.46}$$

so that the test statistics of Equation 3.44 is

$$T_R = (1+\rho)R_s + (1-\rho)R_d. \tag{3.47}$$

Now we can compute the probabilities of false alarm and detection for Equation 3.44. The probability of false alarm can be obtained as

$$P_{FA_{GLRT2_T}} = P\left[T_R|H_0 > \gamma_2'\right] = P\left[\sum_{k=1}^{2} c_k\chi_2^2 > \gamma_2'\right], \tag{3.48}$$

where $T_R|H_0$ is the test statistics of Equation 3.44 under H_0, $c_1 = 1+\rho$, and $c_2 = 1-\rho$ are the constant coefficients of two independent χ_2^2 random variables. By the theorem for finite linear combinations of independent central χ^2 probabilities (see Appendix-B, (48)) we obtain the probability of false alarm explicitly as

$$\begin{aligned} P_{FA_{GLRT2_T}} &= F_1(1+\rho, \gamma_2') + F_2(1-\rho, \gamma_2') \\ &= \frac{1+\rho}{2\rho}\exp\left\{-\frac{\gamma_2'}{2(1+\rho)}\right\} - \frac{1-\rho}{2\rho}\exp\left\{-\frac{\gamma_2'}{2(1-\rho)}\right\}. \end{aligned} \tag{3.49}$$

In a similar manner, the probability of detection can be obtained as

$$P_{D_{GLRT2_T}} = P\left[T_R|H_1 > \gamma_2'\right] = P\left[\sum_{k=1}^{2} c_k \chi_2^2(\lambda_k') > \gamma_2'\right], \tag{3.50}$$

where $T_R|H_1$ is the test statistics of Equation 3.44 under H_1, $c_1 = 1+\rho$, $c_2 = 1-\rho$ are the constant coefficients of two independent $\chi_2'^2(\lambda_k')$ distributions with non-centrality parameters $\lambda_1' = \lambda_s$ and $\lambda_2' = \lambda_d$, which are given by Equation 3.45 and Equation 3.46, respectively. The cumulative distribution function of the sum of M independent $\chi_{v_k}^2(\lambda_k)$ with different coefficients is given in Appendix-C, (48). As a consequence, the probability of detection is obtained in analytic form as

$$P_{D_{GLRT2_T}} = \frac{1}{2} + \frac{1}{\pi}\int_0^\infty \frac{\sin\theta(u)}{u\rho(u)} du, \tag{3.51}$$

where

$$\theta(u) = \frac{1}{2}\sum_{k=1}^{2}\left[2\tan^{-1}(c_k u) + \lambda_k c_k u(1+c_k^2u^2)^{-1}\right] - \frac{1}{2}\gamma_2 u,$$
$$\rho(u) = \prod_{k=1}^{2}(1+c_k^2u^2)^{\frac{1}{2}}\exp\left\{\frac{1}{2}\sum_{k=1}^{2}\frac{\lambda_k(c_k u)^2}{(1+c_k^2u^2)}\right\}.$$

3.5.2 Simulation Results and Discussion

Now that the appropriate probabilities for the detectors in consideration have been introduced, we are ready to compare the performance of these detectors. Since GLRT1 and GLRT2 are not optimum detectors, it is necessary to assess the performance loss with respect to NP1

and NP2 which assume perfect knowledge of signal parameters. Thus, we first compare (i) GLRT2 with NP2 and GLRT1 with NP1 to emphasize the behavior of the GLRT detectors with the corresponding upper bound given by the NP detectors with a given set of probability of false alarm (P_{FA}) values. Then, we compare (ii) NP2 with NP1 to emphasize the relative behaviors of the two upper bound detectors; and, (iii) GLRT2 with GLRT1 to show that GLRT2 outperforms GLRT1 when multipath returns are resolvable in time-domain.

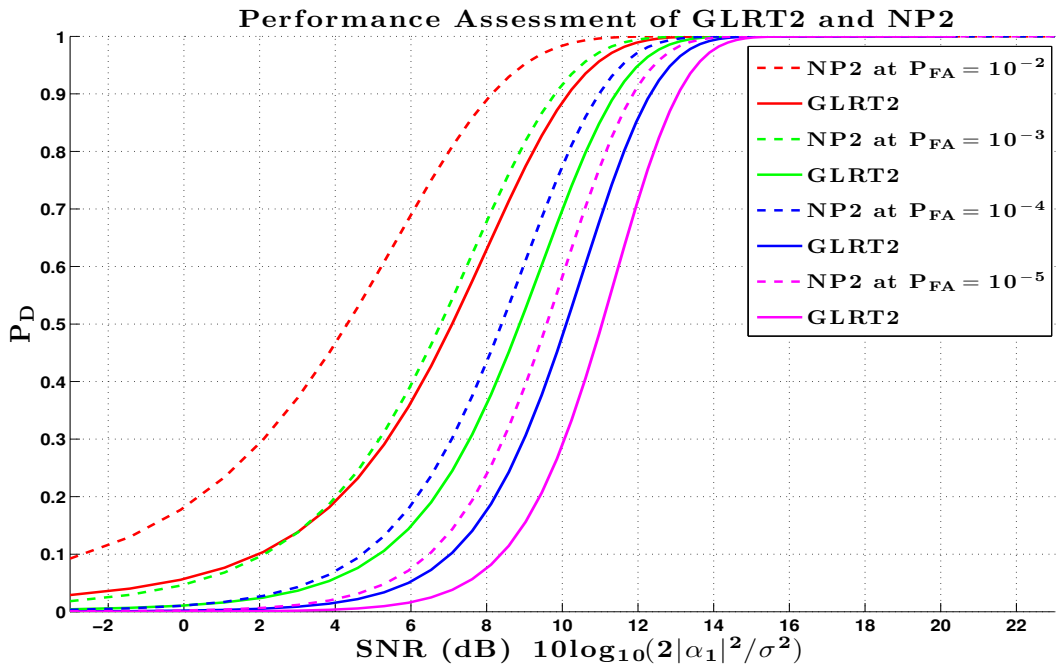

Figure 12. Performance Assessment of GLRT2 with respect to NP2:
Detection performance of GLRT2 Equation 3.24 detector with $P_{D_{GLRT2}}$ Equation 3.36 and NP2 Equation 3.22 clairvoyant detector with $P_{D_{NP2}}$ Equation 3.33.

The performance of the proposed GLRT2 and NP2 are presented in Figure 12. The degradation in detection performance is less than 2 dB in SNR for a low probability of false alarm, *i.e.* $P_{FA} = 10^{-3}$. In practice, imperfect prior knowledge on τ_1 and τ_2 can lead to a further performance loss.

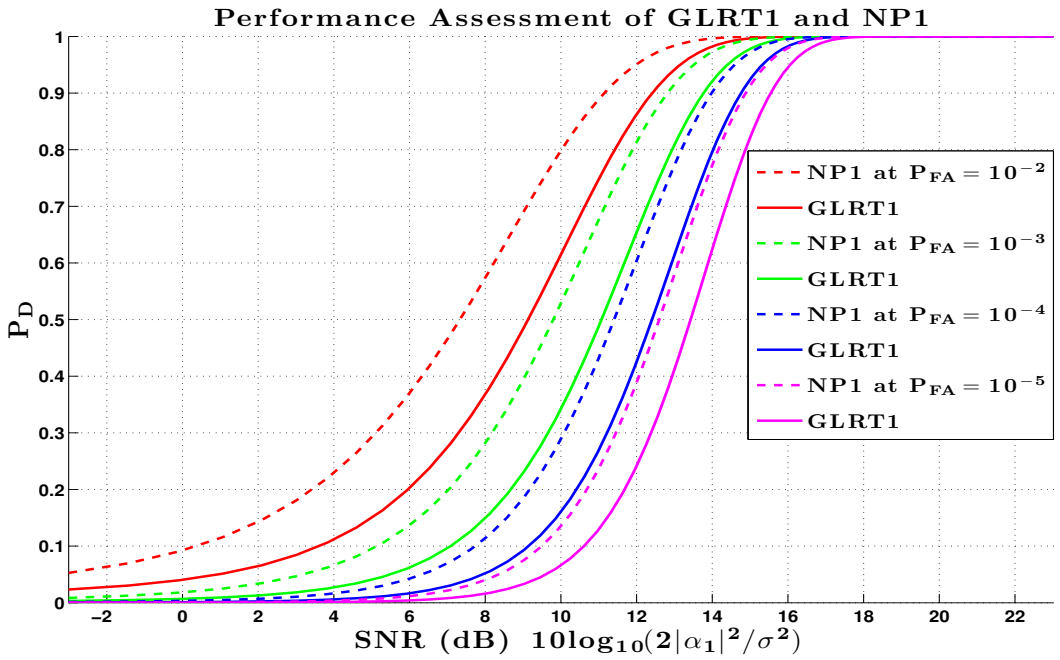

Figure 13. Performance Assessment of GLRT1 with respect to NP1:
Detection performance of GLRT1 Equation 3.18 detector with $P_{D_{GLRT1}}$ Equation 3.30 and NP1 clairvoyant detector Equation 3.17 with $P_{D_{NP1}}$ Equation 3.27.

For the convenience of making a comparison, we provide also in Figure 13 the performance of

the conventional GLRT1 and NP1, which are tested under the same multipath environment as GLRT2 and NP2. The degradation in Figure 13 is 1 dB in SNR for the same $P_{FA} = 10^{-3}$. The fact that the degradation between NP1 and GLRT1 is smaller than the degradation between GLRT2 and NP2 is expected since GLRT2 requires the estimation of two unknown parameters.

3.5.2.1 Performance Comparison in Region-II

The primary goal of this chapter is to show that diverse receiving strategies can be utilized in challenging multipath radar-target environments for better detection performances. In a conventional approach, GLRT1 would be applied for all regions of a radar-target geometry such as those described in this chapter. In the proposed approach, NP1 and GLRT1 are devised as optimum and sub-optimum detectors in Region-I only, whereas NP2 and GLRT2 are devised as optimum and sub-optimum detectors in Region-II. Thus it is important to assess the performance improvement of (i) NP2 relative to NP1; and, (ii) GLRT2 relative to GLRT1, particularly when multipath returns are resolvable as in Region-II.

In Figure 14 we compare NP2 and NP1 for various values of the ratio λ_2/λ_1 with respect to the SNR value of the direct path return, namely SNR $= 10\log_{10} 2|\tilde{\alpha}_1|^2/\sigma^2$. Both receivers are tested under the same multipath environment. Despite of NP1, NP2 exploits the reflected path return which is assumed to be proportional to the direct path strength. Thus, Figure 14 assesses the quantitative measure of the optimal performance improvement of the receiver that exploits multipath compared to the traditional receiver that relies on the direct path return only. We observe that (i) the performance of NP2 is always superior to the one of NP1 that the improvement amount depends upon the ratio λ_2/λ_1 between the multipath returns; and,

(ii) their performance merges when the second path return is weak compared to the direct path return, *i.e.* $\lambda_2 = 0.01\lambda_1$.

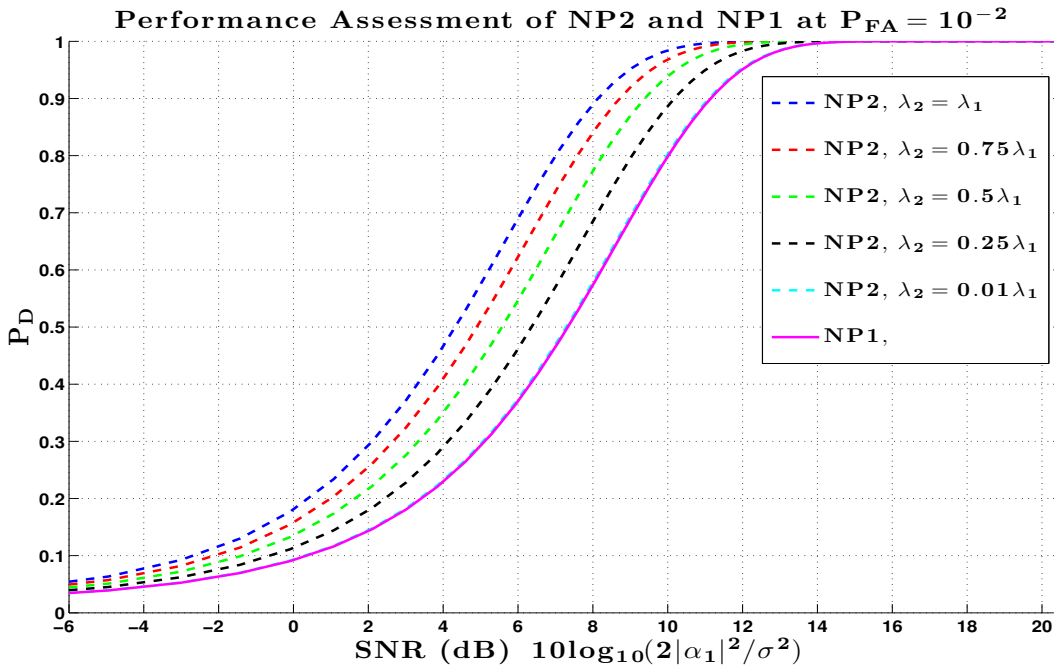

Figure 14. Performance Assessment of NP2 and NP1 at $P_{FA} = 10^{-2}$: Detection performance of detectors NP2 Equation 3.22 with $P_{D_{\mathbf{NP2}}}$ Equation 3.33 and NP1 Equation 3.17 with $P_{D_{\mathbf{NP1}}}$ Equation 3.27 for various values of the ratio $\frac{\lambda_2}{\lambda_1} = \frac{|\tilde{\alpha}_2|^2}{|\tilde{\alpha}_1|^2}$.

In Figure 15 we compare sub-optimum receivers GLRT2 and GLRT1, under the same multipath environment, with respect to the SNR value of the direct path return. In general, the performance of GLRT2 is also superior to the one of GLRT1, depending upon the SNR value of the multipath returns. However, GLRT1 outperforms GLRT2 when the second path return is weak compared to the direct path return. This is well understandable because GLRT2 has an extra cost of estimating a second unknown parameter, which requires a certain level of SNR.

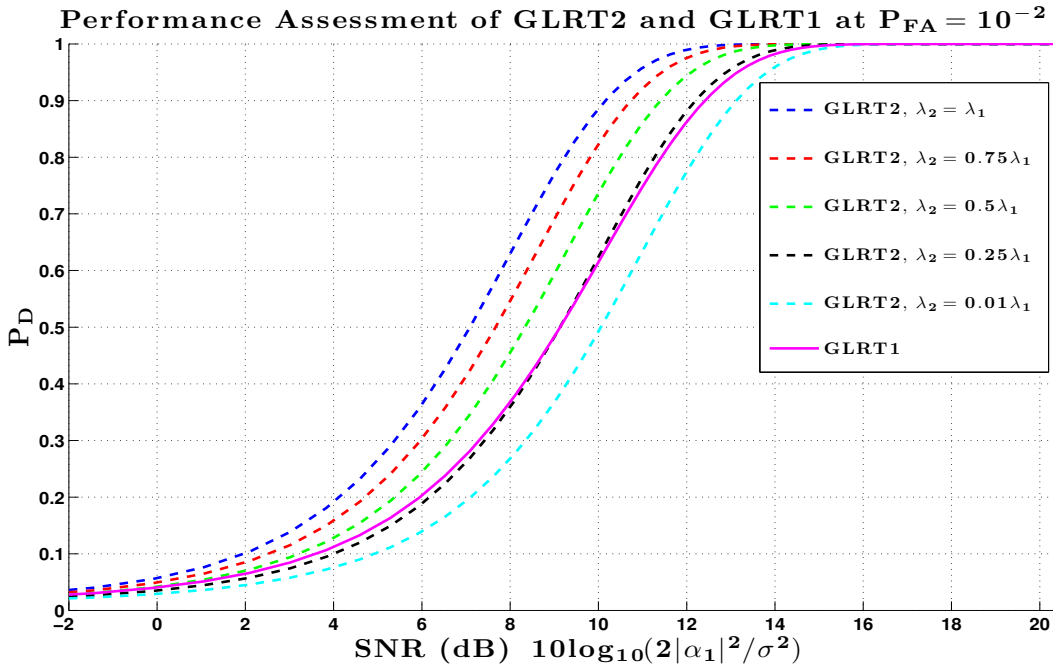

Figure 15. Performance Assessment of GLRT2 and GLRT1 at $P_{FA} = 10^{-2}$: Detection performance of detectors GLRT2 Equation 3.24 with $P_{D_{GLRT2}}$ Equation 3.36, and GLRT1 Equation 3.18 with $P_{D_{GLRT1}}$ Equation 3.30 for various values of the ratio $\frac{\lambda_2}{\lambda_1} = \frac{|\tilde{\alpha}_2|^2}{|\tilde{\alpha}_1|^2}$.

In Figure 16 we present another comparison for a lower value of the probability of false alarm, in order to emphasize that GLRT2 outperforms GLRT1 unless $\lambda_2 \ll \lambda_1$. One can observe that (i) for lower values of the probability of false alarm it is even more evident that GLRT2 outperforms GLRT1; and, (ii) the probability of detection is reduced when the probability of false alarm is reduced, which is a general trend.

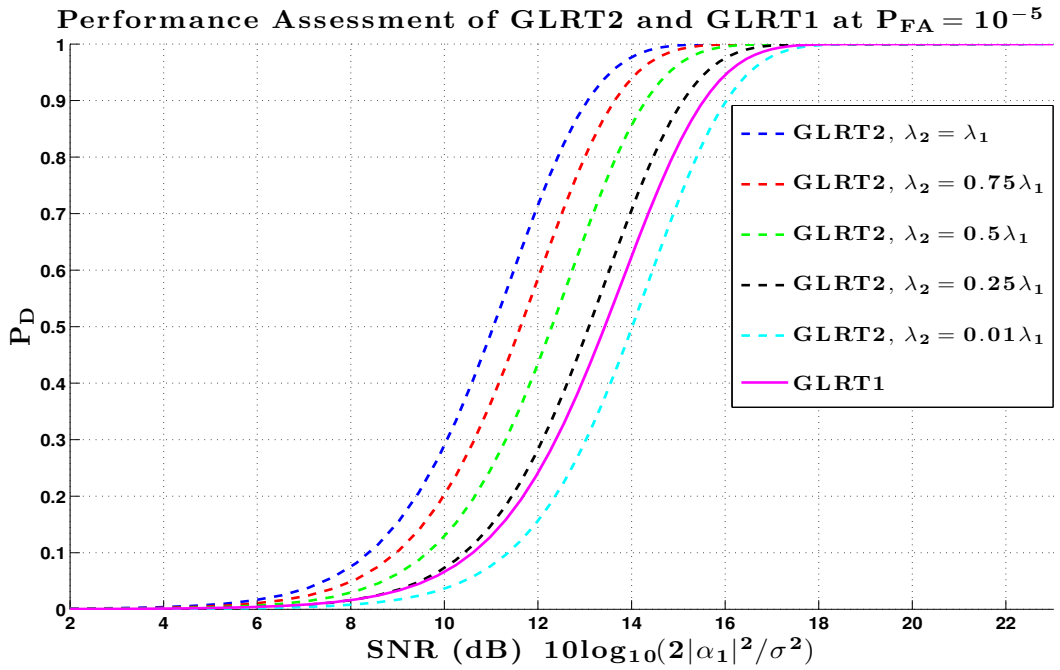

Figure 16. Performance Assessment of GLRT2 and GLRT1 at $P_{FA} = 10^{-5}$: Detection performance of detectors GLRT2 Equation 3.24 with $P_{D_{GLRT2}}$ Equation 3.36 and GLRT1 Equation 3.18 with $P_{D_{GLRT1}}$ Equation 3.30, for various values of the ratio $\frac{\lambda_2}{\lambda_1} = \frac{|\tilde{\alpha}_2|^2}{|\tilde{\alpha}_1|^2}$.

3.5.2.2 Performance Comparison in the Transition Region

The performance in the Transition Region depends upon the degree of overlap of the multipath returns. Therefore we perform a comparison of the two detection strategies based upon the correlation coefficient of the multipath returns. In the following analysis we assume $|\tilde{\alpha}_1| = |\tilde{\alpha}_2|$, so that direct and reflected path returns have same SNR value, *i.e.* $\lambda_1 = \lambda_2$.

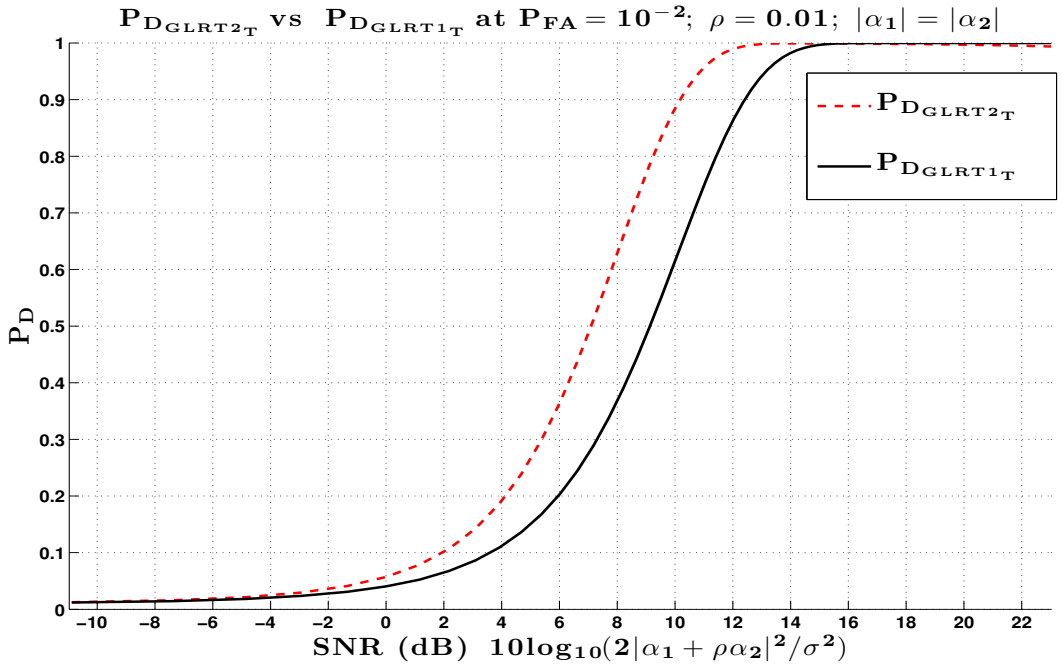

Figure 17. $P_{D_{GLRT2_T}}$ versus $P_{D_{GLRT1_T}}$ when $\rho = 0.01$.

First, we compare the two detectors assuming very low and very high correlation of multipath signal returns: (i) $\rho = 0.01$ and (ii) $\rho = 0.99$. In these two extreme cases, we observe that (1) when the correlation coefficient is very low the signals are essentially distinguishable and the probability of detection behaves similar to what was found in Region-II, as shown in Figure 17; and, (2) when the correlation coefficient is very high then the signals are essentially highly clumped and the probability of detection behaves similar to what was found in Region-I, as shown in Figure 18.

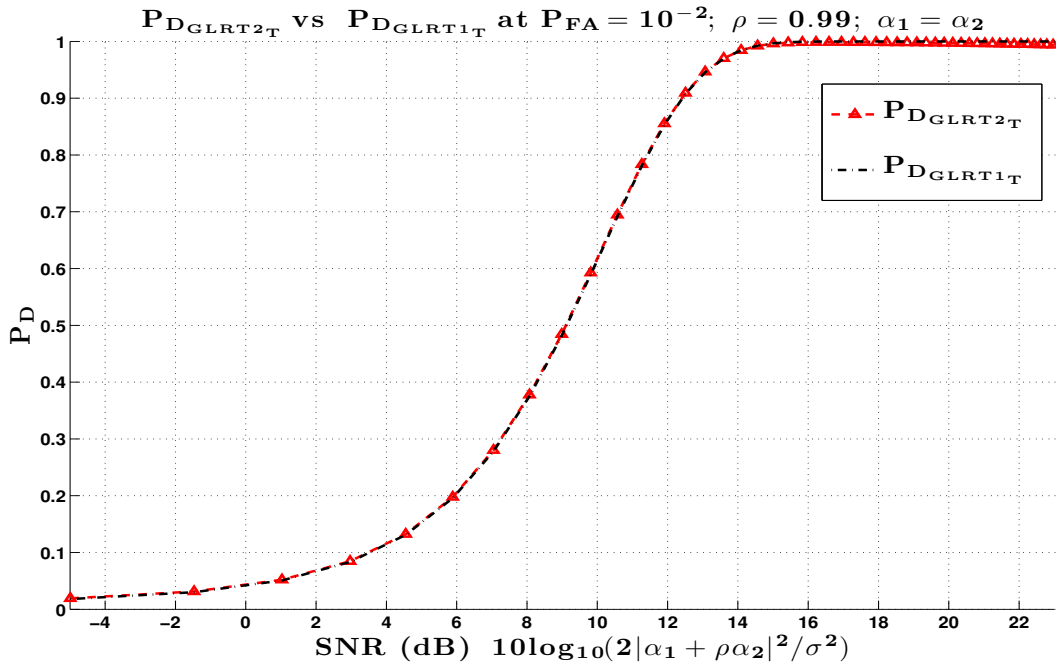

Figure 18. $P_{D_{GLRT2_T}}$ versus $P_{D_{GLRT1_T}}$ when $\rho = 0.99$.

In fact, $\rho = 0.01$ and $\rho = 0.99$ do not belong to the Transition Region but to Region-II and Region-I, respectively. However, it is necessary with Figure 17 and Figure 18 to validate the expressions of the probabilities of false alarm and detection in the Transition Region, *i.e.* Equation 3.39, Equation 3.49 and Equation 3.51.

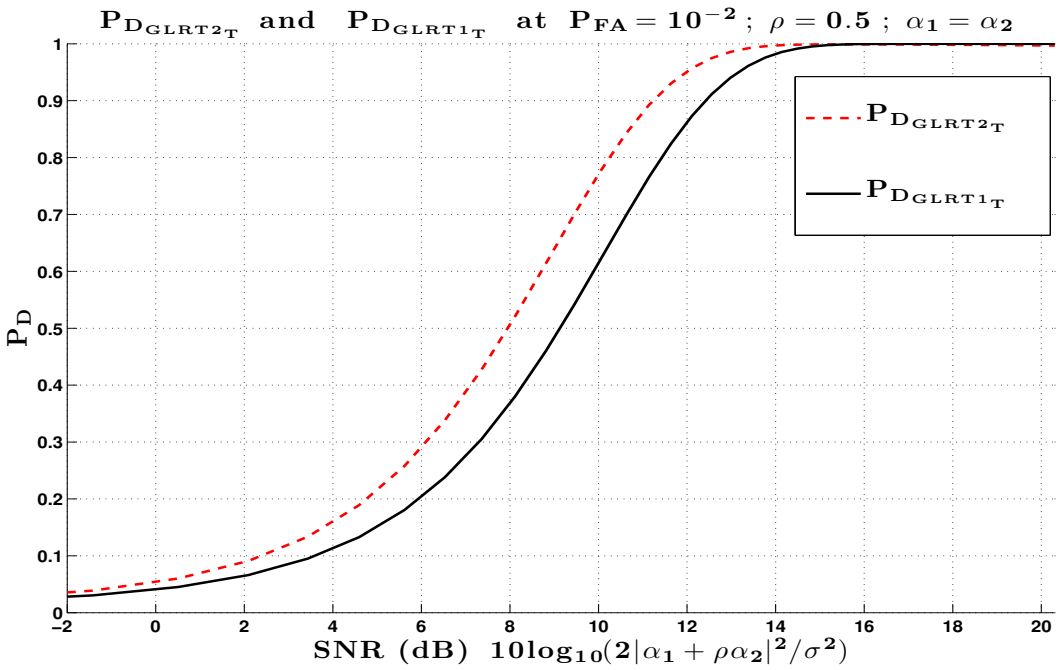

Figure 19. $P_{D_{GLRT2_T}}$ versus $P_{D_{GLRT1_T}}$ when $\rho = 0.5$ and$\tilde{\alpha}_1 = \tilde{\alpha}_2$.

Second, we present the performance of the detectors when $\rho = 0.5$. Our results indicate that the performance of the GLRT2 detector depends on the phase difference between the first

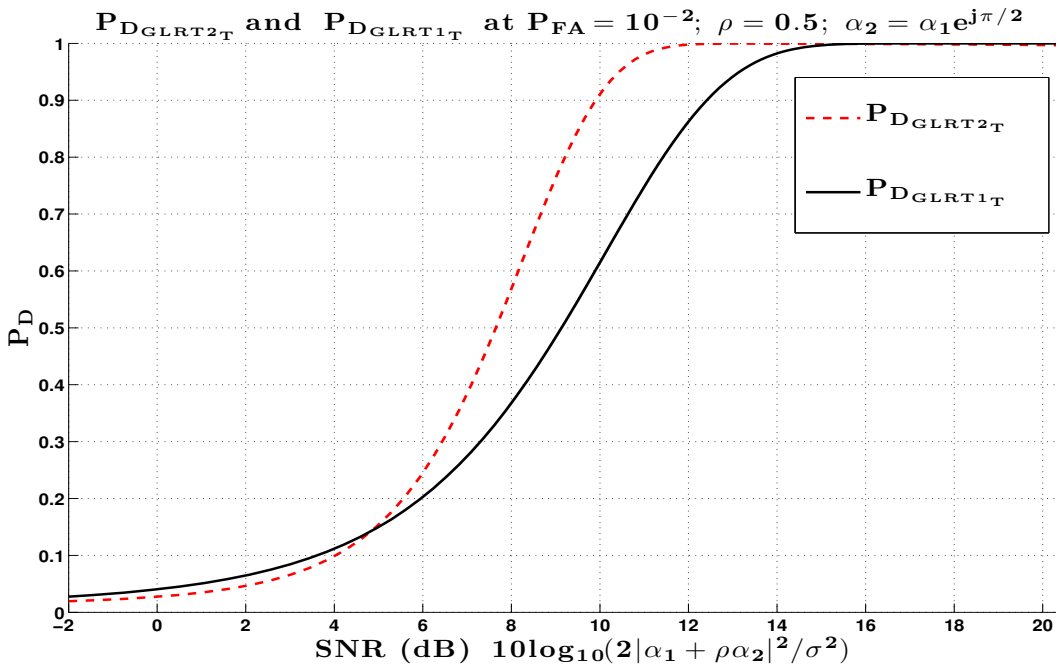

Figure 20. $P_{D_{GLRT2_T}}$ versus $P_{D_{GLRT1_T}}$ when $\rho = 0.5$ and $\tilde{\alpha}_2 = \tilde{\alpha}_1 e^{j\pi/2}$.

and second returns, since the correlation of multipath signal returns are non-negligible. Thus, two extreme situations, in-phase and out-of-phase, are considered in Figure 19 and Figure 20, respectively. When $\tilde{\alpha}_1$ and $\tilde{\alpha}_2$ are in phase, the performance of GLRT2 is always superior to the one of GLRT1, while, when $\tilde{\alpha}_1$ and $\tilde{\alpha}_2$ are out-of-phase, the performance of GLRT2 is only superior to GLRT1 for SNR values above 5 dB. This occurs because GLRT2 is affected by the correlation coefficient since it accounts for two signals, while GLRT1 is independent of the correlation coefficient because it exploits the direct signal only.

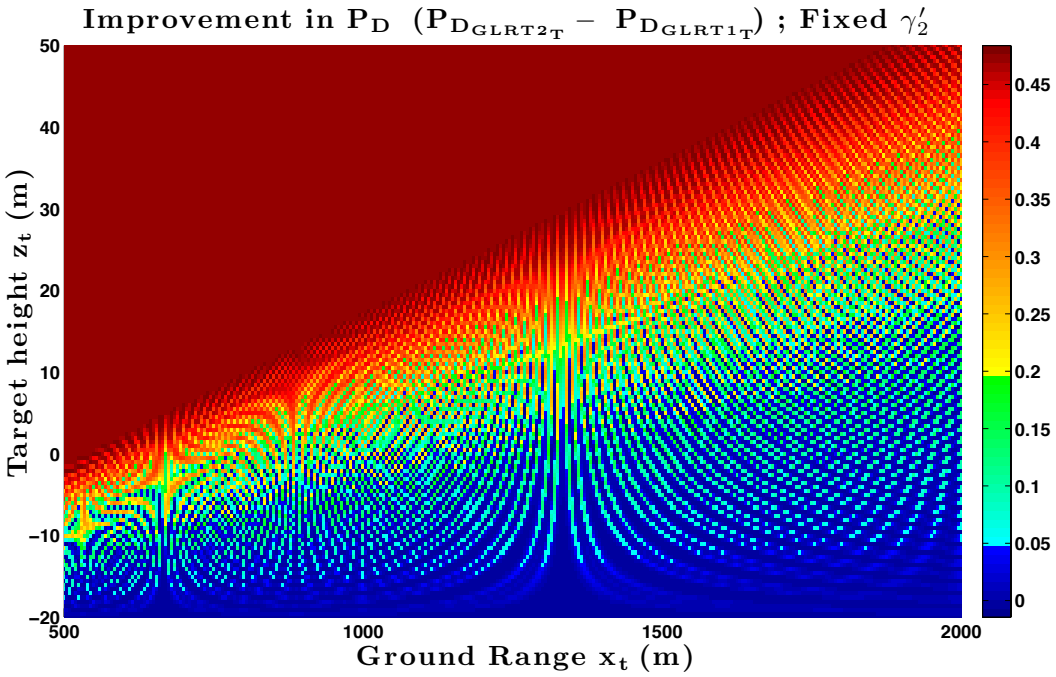

Figure 21. Improvement in P_D $(P_{D_{GLRT2_T}} - P_{D_{GLRT1_T}})$:
The GLRT2 detector threshold γ_2' is fixed when $P_{FA_{GLRT2}} = 10^{-5}$ by Equation 3.35.

In Figure 21, the increase in the target probability of detection, due to the multipath exploited strategy, is presented on a map of the radar-target environment. Constructive and destructive effects of multipath is also shown in the sense of P_D at a certain SNR level. The improvement in the target probability of detection of GLRT2 relative to GLRT1 at any hypothetical target location in the multipath environment is presented when γ_2', which is the threshold for GLRT2, is fixed at $P_{FA_{GLRT2}} = 10^{-5}$ by Equation 3.35. However, $P_{FA_{GLRT2_T}}$ varies across the Transition Region since it depends on ρ as shown in Equation 3.49. Thus, in order to compare two detectors at the same level of P_{FA} we make $P_{FA_{GLRT1_T}} = P_{FA_{GLRT2_T}}$

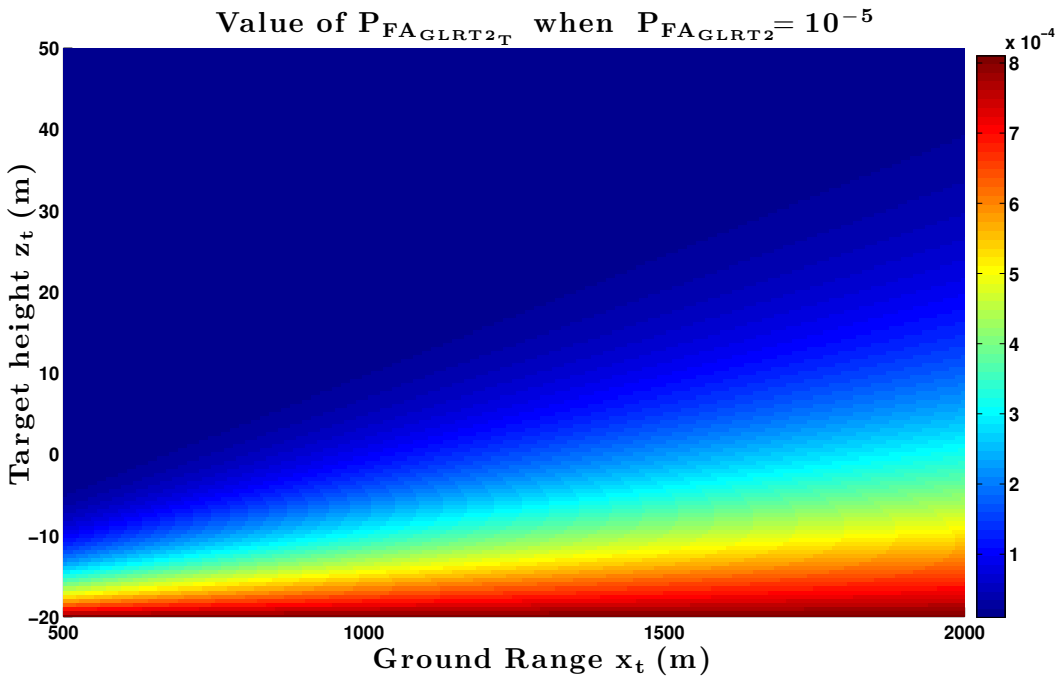

Figure 22. Value $P_{FA_{GLRT2_T}}$ over the Region of Interest when $P_{FA_{GLRT2}} = 10^{-5}$: A map that shows the value of $P_{FA_{GLRT2_T}}$ when GLRT2 threshold γ_2' is set via Equation 3.35 when $P_{FA_{GLRT2}} = 10^{-5}$.

across all regions by changing γ_1' of GLRT1. It is also assumed that $|\tilde{\alpha}_1| = |\tilde{\alpha}_2|$ and SNR $= 10\log_{10}(2|\tilde{\alpha}_1|^2/\sigma^2) = 12$ dB. For the convenience of a complete analysis, in Figure 22 we present the pattern of $P_{FA_{GLRT2_T}}$ across the area of interest with γ_2' set by $P_{FA_{GLRT2}} = 10^{-5}$. It is noted that even if Constant False Alarm Rate (CFAR) property of the GLRT is incorporated to GLRT2 by estimating the noise variance σ^2, GLRT2 would not hold the CFAR property in the transition region since $P_{FA_{GLRT2_T}}$ depends on the correlation coefficient ρ between the multipath returns.

3.5.2.3 Performance Comparison in Region-I

We have not presented a particular performance comparison in Region-I. Rather, in Figure 17 and Figure 21 we have shown that both NP2 and GLRT2 merge to NP1 and GLRT1, respectively, in Region-I.

3.6 Conclusion

We considered the detection of a target by a radar in a multipath environment. We showed that by taking advantage of the multipath it is possible, in general, to increase the probability of detection of the target, compared to a conventional detection problem based on a model of the return signal that accounts only for the direct signal return from the target.

Multipath is accounted for by leveraging on prior knowledge of the environment where the radar operates. Using this prior knowledge and electromagnetic high-frequency ray-tracing analysis, we can predict the time of arrival of each multipath return depending upon the assumed location of the target. In the case study considered, we show that the environment can be divided into three regions: (1) Region-II where multipath components can be clearly distinguished and where the probability of detection is improved by properly accounting for the multipath; (2) Region-I where multipath components cannot be distinguished and there is no possibility of improving the probability of detection; and, (3) the Transition Region where, depending upon the SNR of each individual component and the correlation coefficient of the multipath components, it is possible to improve upon a conventional detector. Thus, it is also shown here that diverse receiving strategies, which are optimum in the particular regions of the multipath environment, can be applied to exploit the best performing receivers.

The performance comparison of two GLRT detectors which are devised based on two extreme cases of a two-ray multipath scenario is presented. GLRT2 assumes that multipath returns are entirely resolvable in time-domain while GLRT1 assumes highly clumped multipath returns in time-domain. It is shown that the performance of GLRT2 depends on the signal strength at the reflected path return as well as the correlation between the direct and reflected path returns.

In the transition region, where multipath returns are neither entirely resolvable nor highly clumped in time-domain, a performance comparison of the GLRT2 and GLRT1 is conducted at various values of correlation coefficient ρ. The probability of detection increase is presented on a map of radar-target environment. Constructive and destructive effects of multipath is also shown in the sense of P_D at a certain SNR level.

We provide a quantitative analysis of the improvement in the target probability of detection by multipath exploitation in the detection strategy assuming a complex Gaussian noise environment. In general, when the signal returns are distinguishable, GLRT2 improves the target probability of detection above GLRT1. This occurs notwithstanding the cost of estimating a second unknown parameter and it requires the strength of the second multipath component to be above a certain threshold.

This chapter provides a method to account for multipath as well as the quantitative analysis of performance increase. The method was explained by referring to a basic case study scenario, however the approach is quite general and it could be extended to more complex environments.

APPENDICES

Appendix A

MATHEMATICAL OPERATIONS ON FISHER INFORMATION MATRIX

A.1 $\underline{\mathbf{J}_{11}}$

From Equation 2.20 one can write

$$\mathbf{J_{11}} = \frac{2}{\sigma^2}\left[\int_0^{T_o}\left|\frac{\partial\tilde{s}_1(t,\mathbf{\Theta})}{\partial\tau_1}\right|^2 + \left|\frac{\partial\tilde{s}_2(t,\mathbf{\Theta})}{\partial\tau_1}\right|^2 + 2\Re\left\{\frac{\partial\tilde{s}_1(t,\mathbf{\Theta})}{\partial\tau_1}\frac{\partial\tilde{s}_2^*(t,\mathbf{\Theta})}{\partial\tau_1}\right\}dt\right] \tag{A.1}$$

We first deal with the first term

$$\begin{aligned}
&\int_0^{T_o}\left|\frac{\partial\tilde{s}_1(t,\mathbf{\Theta})}{\partial\tau_1}\right|^2 dt = \int_0^{T_o}\alpha_1\frac{\partial s(t-\tau_1)}{\partial\tau_1}\left\{\alpha_1\frac{\partial s(t-\tau_1)}{\partial\tau_1}\right\}^* \\
&= |\alpha_1|^2\int_0^{T_o}\frac{\partial s(t-\tau_1)}{\partial\tau_1}\left\{\int_{-\infty}^{\infty}-j2\pi fS(f)e^{j2\pi f(t-\tau_1)}df\right\}^* dt \\
&= |\alpha_1|^2\int_{-\infty}^{\infty}j2\pi fe^{j2\pi f\tau_1}S^*(f)\underbrace{\int_0^{T_o}\frac{\partial s(t-\tau_1)}{\partial\tau_1}e^{-j2\pi ft}dt}_{-j2\pi fe^{-j2\pi f\tau_1}S(f)}df \\
&= |\alpha_1|^2\int_{-\infty}^{\infty}(2\pi f)^2|S(f)|^2df
\end{aligned} \tag{A.2}$$

Appendix A (Continued)

The second term

$$
\begin{aligned}
&\int_0^{T_o} \left| \frac{\partial \tilde{s}_2(t,\mathbf{\Theta})}{\partial \tau_1} \right|^2 dt = \int_0^{T_o} \alpha_2 \frac{\partial s(t-\tau_2)}{\partial \tau_1} \left\{ \alpha_2 \frac{\partial s(t-\tau_2)}{\partial \tau_1} \right\}^* \\
&= |\alpha_2|^2 \int_0^{T_o} \left[\frac{\partial s(t-\tau_2)}{\partial \tau_1} \right. \\
&\quad \left. \times \left\{ \int_{-\infty}^{\infty} -j2\pi f \overbrace{\frac{\tau_1}{\sqrt{\tau_1 + (16 z_t \Delta / c^2)}}}^{F_1 = \partial\tau_2/\partial\tau_1} S(f) e^{j2\pi f(t-\tau_2)} df \right\}^* dt \right] \\
&= |\alpha_2|^2 \int_0^{T_o} \int_{-\infty}^{\infty} \frac{\partial s(t-\tau_2)}{\partial \tau_1} j2\pi f G_1 S^*(f) e^{-j2\pi f(t-\tau_2)} df dt \\
&= |\alpha_2|^2 \int_{-\infty}^{\infty} (j2\pi f) G_1 e^{j2\pi f \tau_2} S^*(f) \underbrace{\int_0^{T_o} \frac{\partial s(t-\tau_2)}{\partial \tau_1} e^{-j2\pi f t} dt}_{(-j2\pi f) G_1 e^{-j2\pi f \tau_2} S(f)} df \\
&= |\alpha_2|^2 G_1^2 \int_{-\infty}^{\infty} (2\pi f)^2 |S(f)|^2 df
\end{aligned}
\tag{A.3}
$$

The third term

$$
\begin{aligned}
&\int_0^{T_o} 2\Re \left\{ \alpha_1 \frac{\partial \tilde{s}_1(t,\mathbf{\Theta})}{\partial \tau_1} \alpha_2^* \frac{\partial \tilde{s}_2^*(t,\mathbf{\Theta})}{\partial \tau_1} \right\} dt \\
&= 2\Re \left\{ \alpha_1 \alpha_2^* \int_0^{T_o} \frac{\partial \tilde{s}_1(t,\mathbf{\Theta})}{\partial \tau_1} \right. \\
&\quad \left. \times \left\{ \int_{-\infty}^{\infty} -j2\pi f \overbrace{\frac{\tau_1}{\sqrt{\tau_1 + (16 z_t \Delta / c^2)}}}^{F_1} S(f) e^{j2\pi f(t-\tau_2)} df \right\}^* \right\} \\
&= 2\Re \left\{ \alpha_1 \alpha_2^* \int_{-\infty}^{\infty} (j2\pi f) G_1 e^{j2\pi f \tau_2} S^*(f) \right. \\
&\qquad \left. \times \underbrace{\int_0^{T_o} \frac{\partial \tilde{s}_1(t,\mathbf{\Theta})}{\partial \tau_1} e^{-j2\pi f t} df}_{(-j2\pi f) e^{-j2\pi f \tau_1} S(f)} dt \right\} \\
&= 2\Re \left\{ \alpha_1 \alpha_2^* \int_{-\infty}^{\infty} (2\pi f)^2 G_1 e^{-j2\pi f(\tau_1 - \tau_2)} |S(f)|^2 df \right\}
\end{aligned}
\tag{A.4}
$$

Appendix A (Continued)

As a result $\mathbf{J}_{11}$ can be written as

$$\mathbf{J}_{11} = \frac{2}{\sigma^2}\Bigg\{ \left(|\alpha_1|^2 + |\alpha_2|^2 G_1^2\right) \int_{-\infty}^{\infty} (2\pi f)^2 |S(f)|^2 df + 2\Re\left\{\alpha_1 \alpha_2^* G_1 \int_{-\infty}^{\infty} (2\pi f)^2 e^{-j2\pi f(\tau_1-\tau_2)} |S(f)|^2 df\right\}\Bigg\} \tag{A.5}$$

A.2 $\underline{\mathbf{J}_{22}}$

In similar manner one can write $\mathbf{J}_{22}$ Equation 2.21 as

$$\mathbf{J}_{22} = \frac{2}{\sigma^2}|\alpha_2|^2 G_2^2 \int_{-\infty}^{\infty} (2\pi f)^2 |S(f)|^2 df \tag{A.6}$$

where

$$G_1 = \frac{\partial \tau_2}{\partial \tau_1} = \frac{\tau_1 + 4\sin\theta h_s/c}{\sqrt{\left(\tau_1 \cos\theta_t\right)^2 + \left(4h_s/c + \tau_1 \sin\theta_t\right)^2}}$$
$$G_2 = \frac{\partial \tau_2}{\partial \theta_t} = \frac{4h_s \tau_1 \cos\theta_t/c}{\sqrt{\left(\tau_1 \cos\theta_t\right)^2 + \left(4h_s/c + \tau_1 \sin\theta_t\right)^2}}.$$

Appendix A (Continued)

A.3 $\mathbf{J}_{12}$

$$
\begin{aligned}
\mathbf{J}_{12} &= \frac{2}{\sigma^2}\Re\Bigg\{ \int_0^{T_o} \alpha_2 \frac{\partial s(t-\tau_2)}{\partial \theta_t} \\
&\qquad \times \left[\alpha_1^* \frac{\partial s^*(t-\tau_1)}{\partial \tau_1} + \alpha_2^* \frac{\partial s^*(t-\tau_2)}{\partial \tau_1}\right] dt \Bigg\} \\
&= \frac{2}{\sigma^2}\Re\Bigg\{ \int_0^{T_o} \alpha_2 \alpha_1^* \frac{\partial s(t-\tau_2)}{\partial \theta_t} \frac{\partial s^*(t-\tau_1)}{\partial \tau_1} dt \\
&\qquad + \int_0^{T_o} |\alpha_2|^2 \frac{\partial s(t-\tau_2)}{\partial \theta_t} \frac{\partial s^*(t-\tau_2)}{\partial \tau_1} dt \Bigg\} \\
&= \frac{2}{\sigma^2}\Re\Bigg\{ \alpha_2 \alpha_1^* G_2 \int_{-\infty}^{\infty} (2\pi f)^2 e^{-j2\pi f(\tau_2-\tau_1)} |S(f)|^2 df \\
&\qquad + |\alpha_2|^2 G_1 G_2 \int_{-\infty}^{\infty} (2\pi f)^2 |S(f)|^2 df \Bigg\}.
\end{aligned}
\tag{A.7}
$$

Appendix A (Continued)

A.4 $\underline{J_{13}}$

From Equation 2.29 we can write that

$$
\begin{aligned}
J_{13} &= \frac{2}{\sigma^2}\Re\Bigg\{ \int_0^{T_0} s(t-\tau_1)\left(\alpha_1 \frac{\partial s(t-\tau_1}{\partial \tau_1}\right)^* dt \\
&\qquad + \int_0^{T_0} s(t-\tau_1)\left(\alpha_2 \frac{\partial s(t-\tau_2}{\partial \tau_1}\right)^* dt \Bigg\} \\
&= \frac{2}{\sigma^2}\Re\Bigg\{ \alpha_1^* \int_0^{T_0} s(t-\tau_1) \int_\infty^\infty j2\pi f S^*(f) e^{-j2\pi f(t-\tau_1)} df\, dt \\
&\quad + \alpha_2^* \int_0^{T_0} s(t-\tau_1) \int_\infty^\infty j2\pi f G_1 S^*(f) e^{-j2\pi f(t-\tau_2)} df\, dt \Bigg\} \\
&= \frac{2}{\sigma^2}\Re\Bigg\{ \alpha_1^* \int_\infty^\infty j2\pi f e^{j2\pi f\tau_1} S^*(f) \underbrace{\int_0^{T_0} s(t-\tau_1) e^{-j2\pi ft} dt}_{e^{-j2\pi f\tau_1} S(f)}\, df \\
&\quad + \alpha_2^* \int_\infty^\infty j2\pi f G_1 e^{j2\pi f\tau_2} S^*(f) \underbrace{\int_0^{T_0} s(t-\tau_1) e^{j2\pi ft} df}_{e^{-j2\pi f\tau_1} S(f)}\, dt \Bigg\} \\
&= \frac{2}{\sigma^2}\Re\Bigg\{ \alpha_1^* \int_\infty^\infty j2\pi f |S(f)|^2 df \\
&\qquad + \alpha_2^* G_1 \int_\infty^\infty j2\pi f e^{-j2\pi f(\tau_1-\tau_2)} |S(f)|^2 df \Bigg\}.
\end{aligned}
\tag{A.8}
$$

Appendix A (Continued)

A.5 $\underline{J_{15}}$

$$
\begin{aligned}
J_{15} &= -E\left[\frac{\partial^2 \ln \mathbf{\Lambda}[r_t, \mathbf{\Theta}]}{\partial\tau_1 \partial\sigma^2}\right] \\
&= -E\left[\frac{\partial}{\partial\sigma^2}\frac{2}{\sigma^2}\Re\left\{\int_0^{T_0}\{r_t - [\tilde{s}_1(t,\mathbf{\Theta}) + \tilde{s}_2(t,\mathbf{\Theta})]\}\right.\right. \\
&\qquad\left.\left.\times \frac{\partial}{\partial\tau_1}[\tilde{s}_1(t,\mathbf{\Theta}) + \tilde{s}_2(t,\mathbf{\Theta})]^* dt\right\}\right] \qquad \text{(A.9)} \\
&= -E\left[-\frac{2}{\sigma^4}\Re\left\{\int_0^{T_0}\{r_t - [\tilde{s}_1(t,\mathbf{\Theta}) + \tilde{s}_2(t,\mathbf{\Theta})]\}\right.\right. \\
&\qquad\left.\left.\times \frac{\partial}{\partial\tau_1}[\tilde{s}_1(t,\mathbf{\Theta}) + \tilde{s}_2(t,\mathbf{\Theta})]^* dt\right\}\right] = 0.
\end{aligned}
$$

Appendix B

FINITE LINEAR COMBINATIONS OF χ^2 PROBABILITIES

Suppose constant coefficients $c_1 > c_2 > \cdots > c_m > 0$.

Theorem: If $\gamma > 0$, then

$$P\left[\sum_{k=1}^{m} c_k \chi^2_{2v_k} \ > \ \gamma\right] = \sum_{k=1}^{m} \frac{1}{(v_k - 1)!} \left[\frac{\partial^{v_k - 1}}{\partial c^{v_k - 1}} F_k(c, \gamma)\right]_{c=c_k} \tag{B.1}$$

where

$$F_k[c, \gamma] = c^{n-1} \exp\{-\gamma/(2c)\} \prod_{r=1, r\neq k}^{m} (c - c_r)^{-v_r}, \tag{B.2}$$

where $n = \sum_{k=1}^{m} v_k$.

Appendix C

CUMULATIVE DISTRIBUTION FUNCTION OF THE LINEAR COMBINATION OF INDEPENDENT $\chi^2_{V_K}(\lambda_K)$

$$P\left[\sum_{k=1}^{m} c_k \chi^2_{v_k}(\lambda_k) > \gamma\right] = \frac{1}{2} + \frac{1}{\pi}\int_0^\infty \frac{\sin\theta(u)}{u\rho(u)}du \tag{C.1}$$

where

$$\begin{aligned}\theta(u) &= \frac{1}{2}\sum_{k=1}^{m}\left[v_k \tan^{-1}(c_k u) + \lambda_k c_k u(1+c_k^2u^2)^{-1}\right] - \frac{1}{2}\gamma u \\ \rho(u) &= \prod_{k=1}^{m}(1+c_k^2u^2)^{\frac{1}{4}v_k}\exp\left\{\frac{1}{2}\sum_{k=1}^{m}\frac{\lambda_k(c_k u)^2}{(1+c_k^2u^2)}\right\}\end{aligned} \tag{C.2}$$

CITED LITERATURE

1. M. I. Skolnik (Ed.), *Radar Handbook,* The McGraw-Hill Companies, 2008.

2. F. E. Nathanson, J. P. Reilly, M. N. Cohen, *Radar Desing Principles, Signal Processing and the Environment,* Mendham, New Jersey: Scitech Publishing, 1999.

3. S. Benedetto and E. Biglieri, *Principles of Digital Transmission with Wireless Applications*, ch.13. New York: Kluwer Academic Publishers, 2002.

4. W. L. Melvin "Space-time adaptive radar performance in heterogenous clutter," *IEEE Trans. Aerospace and Electronic Systems*, vol. 36, no. 2, pp. 621-633, Apr. 2000.

5. F. Gini (Ed.) "Knowledge-based sytems for adaptive radar: Detection, tracking and classification," *IEEE Signal Processing Magazine*, vol. 23, no. 1, pp. 14-76, Jan. 2006.

6. F. C. Robey, D. R. Fuhrmann, E. J. Kelly, R. Nitzberg, "A CFAR adaptive matched filter detector, *Aerospace and Electronic Systems, IEEE Trans. on*, vol. 28, no. 1, pp. 208-216, Jan 1992.

7. E. Conte, A. De Maio, G. Ricci, "GLRT-based adaptive detection algorithms for range-spread targets, *Signal Processing, IEEE Trans on*, vol. 49, no. 7, pp. 1336-1348, Jul 2001.

8. A. De Maio, A. Farina, M. Wicks, "KB-GLRT: exploiting knowledge of the clutter ridge in airborne radar, *Radar, Sonar & Navigation, IEE Proceedings*, vol. 152, no. 6, pp. 421- 428, 9 Dec. 2005.

9. A. De Maio, A. Farina, G. Foglia, "Design and experimental validation of knowledge-based constant false alarm rate detectors," *Radar, Sonar & Navigation, IET*, vol. 1, no. 4, pp. 308-316, Aug. 2007.

CITED LITERATURE (Continued)

10. A. De Maio, A. Farina, G. Foglia, "Knowledge-Aided Bayesian Radar Detectors & Their Application to Live Data," *Aerospace and Electronic Systems, IEEE Trans. on*, vol. 46, no. 1, pp. 170-183, Jan. 2010.

11. J. R. Guerci, and W. L. Melvin (Eds.) "Special section on knowledge-aided sensor signal and data processing," *IEEE Trans. Aerospace and Electronic Systems*, vol. 42, no. 3, pp. 983-1120, July 2006.

12. T. Dogaru, C. Le, "Recent investigations in sensing through the wall radar modeling," *Antennas and Propagation Society International Symposium, AP-S 2008 IEEE,* pp. 1-4, 5-11 July 2008.

13. T. Dogaru, A. Sullivan, C. Kenyon, C. Le, "Radar Signature Prediction for Sensing-through-the-Wall by Xpatch and AFDTD," *High Performance Computing Modernization Program Users Group Conference (HPCMP-UGC), 2009 DoD,* pp. 339-343, 15-18 June 2009.

14. T. Dogaru, A. Sullivan, C. Le, C. Kenyon, , "Radar Signature Prediction for Sensing-Through-the-Wall by Xpatch and AFDTD - Part II," *High Performance Computing Modernization Program Users Group Conference (HPCMP-UGC), 2010 DoD,* pp. 401-406, 14-17 June 2010.

15. T. Dogaru, C. Le, "SAR Images of Rooms and Buildings Based on FDTD Computer Models," *Geoscience and Remote Sensing, IEEE Trans. on,* vol. 47, no. 5, pp. 1388-1401, May 2009.

16. D. K. Barton "Low-Angle Radar Tracking," *Proceedings of IEEE,* vol. 62, no. 4, pp. 687-704, June 1974.

17. W. D. White "Low-Angle Radar Tracking in the Presence of Multipath," *IEEE Trans. on Aerospace and Electronics Systems,* vol. 40, no. 6, pp. 835-852, November 1974.

18. S. Haykin, "*Where do we stand on high resolution in low-angle tracking radar,*" Communications Research Laboratory (Hamilton, Canada), Report 205, August, 1988.

19. T. Lo, J. Litva "Use of a highly deterministic multipath signal model in low-angle tracking," *IEE Proceedings-F,* vol. 138, no. 2, pp. 163-171, April 1991.

CITED LITERATURE (Continued)

20. E. Bosse, R. M. Turner, M. Lecours "Tracking Swerling Fluctuating Targets at Low Altitude over the Sea," *IEEE Trans. on Aerospace and Electronic Systems,*, vol. 27, no. 5, pp. 806-821, Sept. 1991.

21. E. Bosse, R. M. Turner, D. Brookes "Improved radar tracking using a multipath model: maximum likelihood compared with eigen vector analysis," *IEE Proc. Radar, Sonar and Navigation,* vol. 141, no. 4, pp. 213-222, August 1994.

22. S. M. Sherman "The use of complex indicated angles in monopulse radar to locate unresolved targets," *Proc. National Electronics Conference,* 22, pp. 243-248, 1966.

23. S. M. Sherman "Complex indicated angles applied to unresolved radar targets and multipath," *IEEE Trans. on Aerospace and Electronic Systems,* vol. 7, no. 1, pp. 160-170, Jan. 1971.

24. J. Durek, Multipath Exploitation Radar Industry Day. Strategic Technology Office, DAPRA [Online]. Available: http://www.darpa.mil/ STO/ Solicitations/BAA09-01/presentations/MERIndustryDay.pdf

25. J. L. Krolik, J. Farrell, A. Steinhardt, "Exploiting multipath propagation for GMTI in urban environments," *Radar Conference (RADAR), 2006 IEEE*, pp. 24-27, April 2006.

26. R. Linnehan, J. Schindler, "Multistatic scattering from moving targets in multipath environments," *Radar Conference (RADAR), 2009 IEEE,* pp. 1-6, 4-8 May 2009.

27. R. Linnehan, J. Schindler, "Validating multipath responses of moving targets through urban environments," *Radar Conference (RADAR), 2010 IEEE,* pp. 1036-1041, 10-14 May 2010.

28. R. Linnehan, R. Deming, J. Schindler, "Multipath analysis of dismount radar responses," *Radar Conference (RADAR), 2011 IEEE,* pp. 474-479, 23-27 May 2011.

29. B. Chakraborty, Y. Li, J.J. Zhang, T. Trueblood, A. Papandreou-Suppappola, D. Morrell, "Multipath exploitation with adaptivewaveform design for tracking in urban terrain," *Acoustics Speech and Signal Processing (ICASSP), 2010 IEEE International Conference on*, pp. 3894-3897, 14-19 March 2010.

CITED LITERATURE (Continued)

30. J. Yuanwei, J. M. F. Moura, N. O'Donoughue, J. Harley, "Single antenna time reversal detection of moving target, *Acoustics Speech and Signal Processing (ICASSP), 2010 IEEE International Conference on,* pp. 3558-3561, 14-19 March 2010.

31. E. J. Baranoski, "Through-wall imaging: Historical perspective and future directions," *Journal of the Franklin Institute,* vol. 345, no. 6, pp. 556-569, Sept. 2008.

32. P. Setlur, M. G. Amin, F. Ahmad, "Multipath Model and Exploitation in Through-the-Wall and Urban Radar Sensing," *IEEE Trans. Geoscience and Remote Sensing,* vol. 49, no. 10, pp. 4021-4034, Oct. 2011.

33. P. Setlur, G. E. Smith, F. Ahmad, M. G. Amin, "Target Localization with a Single Sensor via Multipath Exploitation, *IEEE Trans. Aerospace and Electronic Systems*, accepted.

34. D. Deiana, A. S. Kossen, W. L. van Rossum, "Multipath exploitation in an urban environment using a MIMO surveillance radar, *Radar Symposium (IRS), 2010 11th International*, pp. 1-4, 16-18 June 2010.

35. V. Krishnan, B. Yazici, "Synthetic aperture radar imaging exploiting multiple scattering," *Inverse Problems*, vol. 27, no. 5, 055004, May 2011.

36. H. T. Hayvaci, A. De Maio, D. Erricolo, "Diversity in receiving strategies based on time-delay analysis in the presence of multipath," *Radar Conference (RADAR), 2011 IEEE*, pp. 1040-1045, 23-27 May 2011.

37. H. T. Hayvaci, A. De Maio, D. Erricolo, "Diversity in receiving strategies based on time-delay analysis in the presence of multipath," *2011 IEEE International Symposium on Antennas and Propagation and USNC/URSI National Radio Science Meeting*, Spokane, Washington, USA, July 3-8, 2011.

38. H. T. Hayvaci, A. De Maio, D. Erricolo, "Performance Analysis of Diverse GLRT Detectors in the Presence of Multipath," *Radar Conference (RADAR), 2012 IEEE*, 7-11 May 2012.

39. H. T. Hayvaci, P. Setlur, N. Devroye, D. Erricolo, "Maximum Likelihood Time Delay Estimation and Cramér-Rao Bounds for Multipath Exploitation," *Radar Conference (RADAR), 2012 IEEE*, 7-11 May 2012.

CITED LITERATURE (Continued)

40. H. T. Hayvaci, A. De Maio, D. Erricolo, Improved Detection Probability of a Radar Target in the Presence of Multipath with Prior Knowledge of the Environment, *Radar, Sonar & Navigation, IET*, submitted.

41. D. Erricolo and P. L. E. Uslenghi, "Two-dimensional simulator for propagation in urban environments," *IEEE Trans. on Vehicular Technology*, vol. 50, no. 4, pp. 1158-1168, July 2001.

42. D. Erricolo, G. D'Elia, and P. L. E. Uslenghi, "Measurements on scaled models of urban environments and comparisons with ray-tracing propagation simulation," *IEEE Trans. Antennas Propag.*, vol. 50, no. 5, pp. 727–735, May 2002.

43. D. Erricolo, U. G. Crovella, and P. L. E. Uslenghi, "Time-domain analysis of measurements on scaled urban models with comparisons to ray-tracing propagation simulation," *IEEE Trans. Antennas Propag.*, vol. 50, no. 5, pp. 736–741, May 2002.

44. E. Conte, A. De Maio, and C. Galdi, "Signal Detection in Compound-Gaussian Noise: Neyman-Pearson and CFAR Detectors," *IEEE Trans. Signal Processing*, vol. 48, no. 2, pp. 419–428, Feb 2000.

45. H. L. Van Trees, *Detection, Estimation and Modulation Theory*, vol 1. New York: John Wiley & Sons, 2001.

46. S. M. Kay, *Fundamentals of Statistical Signal Processing, Detection Theory*, vol 2. New Jersey: Prentice Hall, 1998.

47. Steven M. Kay, *Fundamentals of Statistical Signal Processing, Estimation Theory*, vol 1. New Jersey: Prentice Hall, 1993.

48. J. P. Imhof, "Computing the Distribution of Quadratic Forms in Normal Variables," *Biometrika*, vol. 48, no. 3/4, 417-426, Dec 1961.

49. D. Erricolo, U. G. Crovella, and P. L. E. Uslenghi, "Time-domain analysis of measurements on scaled urban models with comparisons to ray-tracing propagation simulation," *IEEE Trans. Antennas Propag.*, vol. 50, no. 5, pp. 736–741, May 2002.

50. M. Sahmoudi, M. G. Amin, "Fast Iterative Maximum-Likelihood Algorithm (FIMLA) for Multipath Mitigation in the Next Generation of GNSS Receivers," *IEEE Trans. on Wireless Communications,* vol. 7, no. 11, pp. 4362-4374, November 2008.

CITED LITERATURE (Continued)

51. H. L. Van Trees, *Detection, Estimation and Modulation Theory*, vol 1. New York: John Wiley & Sons, 2001.

52. Steven M. Kay, *Fundamentals of Statistical Signal Processing, Estimation Theory*, vol 1. New Jersey: Prentice Hall, 1993.

53. E. Weinstein, A. Weiss, "Fundamental limitations in passive time-delay estimation–Part II: Wide-band systems," *Acoustics, Speech and Signal Processing, IEEE Trans. on,* vol. 32, no. 5, pp. 1064- 1078, Oct 1984.

54. C Le, T. Dogaru, Lam Nguyen, M. A. Ressler, "Ultrawideband (UWB) Radar Imaging of Building Interior: Measurements and Predictions," *Geoscience and Remote Sensing, IEEE Trans. on,* vol. 47, no. 5, pp.1409-1420, May 2009.

55. A. Weiss, E. Weinstein, "Fundamental limitations in passive time delay estimation–Part I: Narrow-band systems," *Acoustics, Speech and Signal Processing, IEEE Trans. on,* vol. 31, no. 2, pp. 472- 486, Apr 1983.

56. E. Weinstein, A. Weiss, "Fundamental limitations in passive time-delay estimation–Part II: Wide-band systems," *Acoustics, Speech and Signal Processing, IEEE Trans. on,* vol. 32, no. 5, pp. 1064- 1078, Oct 1984.

57. P. Stoica, A. L. Swindlehurst, "Maximum likelihood methods in radar array signal processing," *Proceedings of the IEEE,* vol. 86, no. 2, pp. 421-441, Feb 1998.

VITA

NAME:	Harun Taha Hayvaci
EDUCATION:	Ph.D. Student, Electrical and Computer Engineering University of Illinois at Chicago, 2012
	M.S., Electrical and Computer Engineering University of Illinois at Chicago, 2010
	B.A., Electrical and Computer Engineering Bilkent University, Ankara, Turkey 2005
WORK EXPERIENCE:	Research Assistant Department of Electrical and Computer Engineering University of Illinois at Chicago, 2009–2011
	Antenna Design Engineer at PCTEL, Graduate Assistant College of Engineering University of Illinois at Chicago, 2007–Present
	Research Assistant Department of Electrical and Computer Engineering University of Illinois at Chicago, 2006–2007
	Teaching Assistant Department of Electrical and Computer Engineering University of Illinois at Chicago, Fall 2006 and Fall 2007
	Electrical Engineer Intern TRT (Turkish Radio and Television Institution), Ankara, Turkey, 05/2004 - 08/2004
	Teaching Assistant at Analog Electronics Department of Electrical and Electronics Engineering Bilkent University, Ankara, Turkey, 09/2003-01/2004

Vita (Continued)

Electrical Engineer Intern
ASELSAN (Military Electronics Industry), Ankara, Turkey, 08/2003 - 09/2003

AWARDS:

University of Illinois at Chicago Graduate Student Council Travel Award,
Travel fellowship to support conference attendance, 2007, 2009, 2011

University of Illinois at Chicago Graduate College Presenter Award, 2011

The National Academies Travel Fellowship, The National Academies
Travel fellowship to support conference attendance, 07/2007–01/2010

Honor Student Award, Bilkent University, 05/2005

Bilkent University Undergraduate Scholarship, Bilkent University, 2001

PUBLICATIONS:

Journals

H.T. Hayvaci, P. Setlur, N. Devroye, D. Erricolo, "Joint Detection, Estimation and Cramèr-Rao Bounds for Multipath Exploitation", in preparation.

H.T. Hayvaci, A. De Maio, D. Erricolo, "Radar Target Detection in the Presence of Multipath with Prior Knowledge on Multipath Delay Profile," *IET Radar, Sonar & Navigation*, Submitted.

Arindam Das, Harun T. Hayvaci, Manish K. Tiwari, Ilker S. Bayer, Danilo Erricolo, Constantine M. Megaridis, Superhydrophobic and Conductive Carbon Nanofiber/PTFE Composite Coatings for EMI Shielding", *Journal of Colloid Interface Science* 353, pp. 311-315, 2011.

D. Erricolo, S.M. Canta, H.T. Hayvaci, M. Albani, "An experimental validation for the Incremental Theory of Diffraction," *IEEE Trans. on Antennas and Propagation,* Vol. 56, No. 8, Part 2, pp. 2563-2571, Aug. 2008.

Vita (Continued)

Conferences

H.T. Hayvaci, P. Setlur, N. Devroye, D. Erricolo,"Maximum Likelihood Time Delay Estimation and Cramér-Rao Bounds for Multipath Exploitation," *Accepted to Radar Conference (RADAR), 2012 IEEE*, 7-11 May 2012.

H.T. Hayvaci, A. De Maio, D. Erricolo,"Performance Analysis of Diverse GLRT Detectors in the Presence of Multipath," *Accepted to Radar Conference (RADAR), 2012 IEEE*, 7-11 May 2012.

H.T. Hayvaci, A. De Maio, D. Erricolo, "Diversity in receiving strategies based on time-delay analysis in the presence of multipath," *2011 IEEE International Symposium on Antennas and Propagation and USNC/URSI National Radio Science Meeting*, Spokane, Washington, USA, July 3-8, 2011.

H.T. Hayvaci, A. De Maio, D. Erricolo,"Diversity in receiving strategies based on time-delay analysis in the presence of multipath," *Radar Conference (RADAR), 2011 IEEE*, pp.1040-1045, 23-27 May 2011.

H.T. Hayvaci, D. Erricolo, Enhancing Radar Ambiguity Function with Deterministic Propagation Model, *2009 IEEE International Symposium on Antennas and Propagation and USNC/URSI National Radio Science Meeting*, Charleston, SC, USA, June 1-5, 2009.

H.T. Hayvaci, D. Erricolo, D. Tuninetti, M. Rangaswamy, Multistatic Radar: Relation between the Green Function and the Ambiguity Function, *XXIX General Assembly of the International Union of Radio Science*, Chicago, IL, USA, Aug. 7-16, 2008.

L. Lo Monte, H.T. Hayvaci, D. Erricolo, Propagation Model for RF Geotomography, *XXIX General Assembly of the International Union of Radio Science*, Chicago, IL, USA, Aug. 7-16, 2008.

B. Elnour, H.T. Hayvaci, L. Lo Monte, D. Erricolo, "A MIMO Cube Antenna for Communication and Sensing Applications", *2008 IEEE International Symposium on Antennas and Propagation and USNC/URSI National Radio Science Meeting,* San Diego, CA, USA, July 2008.

Vita (Continued)

H.T. Hayvaci, B. Elnour, D. Erricolo, "Design of a Multi-element Multi-polarized Antenna that enables applications based on polarization diversity", *2007 URSI North American Radio Science Meeting URSI-CNC/USNC,* Ottawa, ON, Canada, July 2007.

Stefano Mihai Canta, Harun Taha Hayvaci, Danilo Erricolo, and Matteo Albani, An experimental validation for the Incremental Theory of Diffraction, *2006 IEEE Antennas and Propagation Society International Symposium with on and USNC/URSI National Radio Science and AMEREM Meetings*, Albuquerque, NM, USA, July 2006.